NREL/TP-451-5452 • UC Category: 271 • DE 93017083

Fundamental Studies of Defect Generation in Amorphous Silicon Alloys Grown by Remote Plasma-Enhanced Chemical-Vapor Deposition

Final Subcontract Report
1 July 1989 – 31 December 1992

G. Lucovsky
North Carolina State University
Raleigh, North Carolina

NREL technical monitor: J. Benner

National Renewable Energy Laboratory
1617 Cole Boulevard
Golden, Colorado 80401-3393
Operated by Midwest Research Institute
for the U.S. Department of Energy
under Contract No. DE-AC02-83CH10093

Prepared under Subcontract No. XM-9-18141-2

August 1993

NOTICE

Printed in the United States of America
Available from:
National Technical Information Service
U.S. Department of Commerce
5285 Port Royal Road
Springfield, VA 22161

Price: Microfiche A01
Printed Copy A04

Codes are used for pricing all publications. The code is determined by the number of pages in the publication. Information pertaining to the pricing codes can be found in the current issue of the following publications which are generally available in most libraries: *Energy Research Abstracts (ERA)*; *Government Reports Announcements and Index (GRA and I)*; *Scientific and Technical Abstract Reports (STAR)*; and publication NTIS-PR-360 available from NTIS at the above address.


Printed on recycled paper

DISCLAIMER

Portions of this document may be illegible electronic image products. Images are produced from the best available original document.

Table of Contents

I. SUMMARY OF MAJOR RESEARCH ACCOMPLISHMENTS

The overall objective of this research program has been the reduction of intrinsic bonding defects in amorphous and microcrystalline Si alloys by control of the bonding chemistry and the microstructure via the deposition process reactions. The specific approach has been to use remote plasma-enhanced chemical-vapor deposition, and reactive magnetron sputtering to limit the multiplicity of deposition reaction pathways, and thereby gain increased control over the thin film chemistry and microstructure. The research effort has included i) the deposition of amorphous and microcrystalline Si alloy materials by the remote plasma-enhanced chemical-vapor-deposition, PECVD, process and by reactive magnetron sputtering, and ii) the evaluation of the material properties of these films for potential applications in photovoltaic devices. The focus of the research has been on gaining a fundamental understanding the relationships between deposition reaction pathways, the bonding of dopant and alloy aoms, and the electrical properties of importance for photovoltaic applications. This has involved studying the factors that contribute to defect generation, and to defect removal and/or neutralization. In addition to the experimental studies, the research has also included theoretical and modeling studies aimed at understanding the relationships between local atomic arrangements of Si and alloy atoms, and the electrical, optical, vibrartional and defect properties.

The major research accomplishments to date have been:

- a demonstration that device-quality intrinsic and doped amorphous Si could be produced by the remote PECVD process;
- a demonstration that the remote PECVD process could be extended to the deposition of device-quality microcrystalline Si, μc-Si, films as well;
- the incorporation of device quality intrinsic a-Si and μc-Si, and doped a-Si and μc-Si into TFT device structures, and the indenfication of the factors that contribute to the effective channel mobility; and
- the identification of B-compensated μc-Si, a-Si,O:H and a-Si,N:H alloys, as candidates for the i-region materials in p-i-n PV device structures.

In addition to these accomplishments considerable progress has been made in understanding i) the microscopic transport mechanisms in μc-Si, and the mechanisms contributing to the sub-picosecond photo-transport processes in a-Si:H.

II. TECHNICAL PROGRESS REPORT
RESEARCH ACCOMPLISHMENTS

This part of the report is organized into four sections, each of which describes the progress made in a particular aspect of this research. The following topics are included i) deposition of amorphous and microcrystlline Si alloy films, ii) transport and optical properties, iii) perfromance of device structures, and iv) theory and modelling.

The experimental approach has utilized two deposition techniques i) primarily remote plasma-enhanced chemical-vapor deposition, Remote PEVCVD, and ii) reactive magnetron sputtering, RMS, where appropriate. These techniques generally provide more control over deposition reaction pathways, film composition and local bonding chemistries than the conventional glow discharge, GD, process, and in addition, they have been shown by us to produce films of comparible device-quality -- both undoped and/or intrinsic, and heavily doped n- and p-type. Both processes have also been used to generate microcrystalline, as well as amorphous thin films, μc-Si and a-Si:H, respectively. Property measurements have included i) the temperature-dependent dark conductivity, ii) the photoconductivity, iii) the constant photocurrent method, CPM, iv) IR absorption and Raman scattering, v) optical absorption, vi) minority transport by the optical grating method, and vi) studies of trapping, recombination and transport on femto-second, or sub-pico-second time-scales. The theoretical and modeling studies have been based on two different computational approaches i) the semi-empirical tight-binding method, and ii) ab-initio quantum-chemistry methods.

A. Deposition of a-Si alloy fims by Remote PECVD

A.1. Local Bonding Arrangements of H-atoms in a-Si:H

The total concentration, and the local bonding arragements of H-atoms play important roles in determing the electronic properties of a-Si:H thin film alloy materials. It is therefore important to understand the factors that contribute to i) the concentration of bonded-H, and ii) the distribution of H-atoms between mono- and poly-hydride bonding groups, hereafter, Si-H and Si-H_X, respectively. In addition, it is important to understand the role that H-atoms play in defect relaxation processes that can take place during, or after thin film deposition. In the GD, Remote PECVD, and RMS

processes, H-atom incorporation in electronic-grade materials is determined by surface reactions that occur during film deposition, rather than by homogeneous, or gas-phase reactions in which Si-H molecular structures are formed in the gas phase, and then *condense to form* the deposited film. Under these conditions the concentration of bonded-H is determined by i) a H-atom *availability factor*, which is characteristic of the specific reaction pathways for each deposition process, and ii) the substrate temperature, which determines the *fraction of the available* hydrogen that is retained in the film. The distribution of bonded-H between mono-hydride and poly-hydride groups has been shown to be determined primarily by the total concentration of H-atoms, [H], that are incorporated under a specific set of deposition conditions. Because of this [H] is not a unique function of a single deposition variable such the substrate temperature, T_S.

These aspects of the bonded-H incorporation are illustrated in Figs. 1 and 2, which show the relative concentrations of the mono- and poly-hydride groups in a-Si:H produced by the GD and Remote PECVD processes, respectively, as functions of i) T_S in Figs. 1(a) and (b); and ii) the total H-concentration, [H], in Figs. 2(a) and (b). The solid lines in Figs. 2(a) and (b) are from a statistical model that has been developed by us, and used to compute the probabilities of isolated and connected Si-H surface bonding sites. In the model, these types of surface bonding sites are assumed to be the nucleation centers for the mono- and poly-hydride bonding groups that are eventually in corporated into the thin film structure. The differences between Figs. 1(a) and 1(b) reflect the fact that for T_S in the range between about 100°C and 300°C, the Remote PECVD films have about half of the bonded-H available for film incorporation relative to the GD films. This is a result of the different ways the Si-atom source gas silane, SiH_4, is fragmented and comsumed in the respective film deposition reactions.

Two of the factors that are of importance in device-quality undoped a-Si:H thin films are i) the amount of bonded-H, in particular the local bonding arrangements of the H-atoms, and ii) the substrate temperature. These two aspects of film formation can not be indepedently controlled in the conventional GD process, and as a result of this, a body of experimental data has been developed which links device-quality material to two factors i) a bonded-H concentration of the order of 10 to 15 at.%, and ii) a substrate temperature of approximately 250°C. In the GD deposition process, the substrate temperature, and time required for film deposition, combine to determine the amount of thermal annealing that occurs during film deposition. Thermal annealing

promotes rearrangements in the local atomic bonding that generally serve to reduce the concentration of intrinsic defects such as Si-atom dangling bonds, e.g., as in the removal of photo-induced defects associated with the Stabler-Wronski effect.

a-Si:H produced by Remote PECVD between about 150 and 200°C has superior electrical properties, e.g., photoconductivity, compared to GD material deposited in the same range of T_S. However, the a-Si:H films deposited by Remote PECVD between about 225 and 250°C have essentially the same electrical properties as GD a-Si:H deposited in the same range of T_S. To understand these differences between the two plasma-assisted deposition processes, experiments were perfomed to identify the separate roles of H-atom incorporation, and thermal annealing in promoting defect reduction. a-Si:H films were deposited at ~40°C by RMS with a concentration of bonded-H of approximately 14±3 at.%, and predominantly in mono-hydride, or Si-H bonding groups. The defect concentration was determined by the CPM method. Films were annealed in the dark at temperatures of 150°C, 162°C, 173°C and 240°C, and changes in the conductivity were used to determine the kinetics, in particular, the characteristic annealing time for the relaxation process that resulted in defect reduction. Defect reduction was determined from improvements in the $\eta\mu\tau$ product, as estimated from photoconductivity measurements, and by decreases in the sub-band-gap absorption, as determined by combining CPM and optical absorption data. These experiments showed that i) the incorporation of the *right amount* of bonded-H, ~10-15 at.%, and ii) defect relaxation could either be accomplished during film deposition at ~250°C, as in the GD process, or in two separate steps as in the RMS experiments; i.e., by deposition at 40°C, combined with post-deposition annealing at 175°C to 250°C. Extrapolating these observations to the improved performance of the Remote PECVD films with respect to GD films in the 150-200°C range of T_S, the improved electrical properties of the Remote PECVD films are determined by two factors i) lower bonded-H concentrations, and therefore lower concentrations of H-atoms in poly-hydride groups, and ii) significant annealing and defect relaxation that take place during film deposition at the temperatures between 150 and 200°C. Annealing also takes place in GD films deposited between 150 and 200°C; however, the higher poly-hydride bonding fractions, intrinsic to the deposition process chemistry, generate higher concentrations of defects that cannot be removed by annealing. The kinetics of defect relaxation discussed above are essentially the same as those determined for defect relaxation in light-soaked films; i.e., the Stabler-Wronski effect. This means that the defects associated with the 40°C deposition may

be similar in their microscopic nature to those introduced by light-soaking.

In the course of these studies a new technique was used to extract a characteristic relaxation time from the annealing or light-soaking data. Instead of trying to fit a stretched-exponential function to the entire data set, the data for the changes in the conductivity was analyzed to determine the time at which the relxation was proceeding at the most rapid rate. This time corresponds exactly to the characteristic time in a stretched exponential function. This new process avoids the inherent difficulty of trying to fit the data at long and short times. Generally, both of these regions of a stretched exponential cannot be fit simultaneously, resulting in potential errors in the determination of the relaxation time. The new analytical procedure that we have introduced avoids these problems.

A.2. Doped a-Si films

We had established prior to the begining of this NREL sub-contract that n-type doping of a-Si:H could be accomplished in a Remote PECVD process by supplying the SiH_4 and PH_3 down-stream from the plasma, and using active species, extracted from a remote He plasma, to drive the deposition and doping reactions. We showed i) by AES, that the concentration ratios of P and Si in the deposited films were essentially the same as the gas-phase ratios of their respective source gases, and ii) that the conductivity and activation energies for a given gas ratio of PH_3 to SiH_4 in Remote PECVD, were the same as those reported by Spear and LeComber for GD films using same fractional concentration of the doping gas.

We have extended these studies to p-type doping using B_2H_6 as the source for B, and find essentially the same results as for the n-type dopants, i.e., that the p-type doping of a-Si:H via the Remote PECVD process is equivalent to that of the GD process in the sense that the same gas phase ratios of dopant gas to SiH_4, yield the same electrical properties in the deposited films. This has been confirmed for gas phase ratio varying between approximate 10^{-5} and 10^{-1}. The elecrical properties of the most heavily doped n-type and p-type films are presented in the table below, along with the properties of the as-deposited, or undoped films as a point of reference.

Table I: Electrical Properties of Doped a-Si:H by Remote PECVD

Material	H_2/SiH_4 ratio	Dopant Gas/ SiH_4 ratio	Dark Conductivity (S/cm) $(\Omega cm)^{-1}$	Activation Energy (eV)
a-Si:H	0	0	2.4×10^{-10}	0.80
a-Si:H(n)	0	1×10^{-2}	2.0×10^{-3}	0.25
a-Si:H(p)	0	1×10^{-1}	2.4×10^{-3}	0.31

A.3. Doped Microcrystalline Si (μc-Si)

We have optimized the conditions for deposition of undoped, near-intrinsic and heavily-doped thin films of μc-Si by Remote PECVD. This is achieved at substrate temperature of 250°C, a H_2/SiH_4 flow rate of 30:1, and with the H_2, and the Si-atom and dopant atom source gases injected downstream from the plasma generation region. Conductivities of 50-100 S/cm for n-type material, and 6-10 S/cm for p-type μc-Si, with activations energies of approximately 0.02 eV and 0.04 eV respectively, have been achieved for source gas mixtures of 10^{-2} PH_3/SiH_4 and 10^{-3} B_2H_6/SiH_4, respectively. The electrical properties of these films are displayed in Table II.

From Table II, we see that n-type μc-Si films have been grown from P-atom/Si-atom source gas mixtures up to and including 10^{-2} PH_3/SiH_4, whereas p-type μc-Si films could only be grown from B-atom/Si-atom source gas mixtures to 10^{-3} B_2H_6/SiH_4. Films deposited from B-atom/Si-atom source gas mixtures $>10^{-3}$ B_2H_6/SiH_4 were amorphous as determined by Raman scattering, TEM imaging and electron diffraction.

Table II: Electrical Properties of μc-Si Films by Remote PECVD

Material	H_2/SiH_4	Dopant Gas/	Dark Conductivity	Activation
ratio	SiH_4 ratio		(S/cm) = $(Wcm)^{-1}$	Energy (eV)
μc-Si	30:1	0	6.0×10^{-4}	0.30
μc-Si(N)	30:1	$3x10^{-5}$	0.2	0.08
μc-Si(N)	30:1	$3x10^{-4}$	5.0	0.05
μc-Si(N)	30:1	$1x10^{-2}$	50 - 100	0.02
μc-Si(P)	30:1	$1x10^{-5}$	6.0×10^{-8}	0.70
μc-Si(P)	30:1	$2x10^{-4}$	7.0×10^{-4}	0.24
μc-Si(P)	30:1	$1x10^{-3}$	6 - 10	0.04
a-Si:H(P)	30:1	$1x10^{-2}$	4.0×10^{-5}	0.40
a-Si:H(P)	30:1	$1x10^{-1}$	3.0×10^{-3}	0.30

We have conducted a detailed study of the most-resistive μc-Si. These films are qualitatively different than the undoped films with regard to their photoconductivity, and have opened up what we believe to be interesting new options for device structures. *Boron-compensated* μc-Si thins films were deposited using a 10^{-5} ratio of B_2H_6 to SiH_4. These films displayed dark conductivities as low as 6.0×10^{-8} S/cm with activation energies up to 0.66 eV. These films also have a relatively high photoconductivity, ~10^{-4} S/cm to ~0.5 AM1 white light. The E_{04} band gap was approximately 1.9 eV, as determined by the photon energy at which the absorption constant is 10^4 cm^{-1}. Previous reports had quoted a value of ~1.4 eV; this was in error due to problems with analyzing data in which interference fringes overlapped the absorption edge region. Measurements of the photoconductivity of this B-compensated μc-Si under prolonged light exposure indicated no photodegradation for soaking times up to 40 hours at light levels of ~0.5 AM1.

The dark conductivity of the μc-Si material changes from n-type to B-compensated-intrinsic, and eventually to strongly p-type over a narrow range of B_2H_6 to SiH_4 doping mixtures. *Exact* compensation was difficult to achieve and depended on the recent deposition history of the chamber, which had also been used to deposit

n- and p-type Si and Si,C materials. Attempts to minimize chamber contamination have had only limited success. One aspect of this study examined data from films deposited under identical conditions, but influenced by residual B-doping, and possible P-compensation derived from the chamber walls and fixtures. In this way we have generated a series of B-compensated μc-Si films that display a range of electrical properties that span the region in which exact numerical compensation can occur.

Figure 3(a) displays conductivity and photo-conductivity vs the dark conductivity activation energy, E_σ^*, for B-doped μc-Si. These data show a weak dependence of the photo-conductivity, to 0.5 AM1 white-light exposure, on the dark conductivity activation energy. As E_σ^* increases, the photoconductivity decreases by a relatively small amount compared to the decrease in the dark conductivity for the same change in E_σ^*. There is an inherent ambiguity in these data plotted as a function of the activation energy that derives from the behavior of the conductivity versus doping curves. The conductivity initially drops in the defect-controlled region as diborane is introduced into the source gas mixture. It reaches a minimum when the B-atoms *exactly compensate* the donor-like defects, and then increases again as the material becomes p-type. The *same values* of the dark conductivity and the activation energy can then occur on *both sides* of the conductivity minimum. Specifically, the activation energy first *increases* in the defect-controlled region, and then *decreases* after compensation is exceeded and the material becomes p-type. In order to develop an understanding of the dark conductivity and photoconductivity behaviors on both sides of the compensation point, we have obtained the B-concentrations, [B], on a subset of these films using SIMS, and have replotted the conductivity data in terms of this variable, [B], in Fig. 3(b).

From the variation of dark conductivity with [B] in Fig. 3(b), we observe that the film with the lowest B concentration, ~$3x10^{17}$ cm^{-3}, is an n-type film, in which the native defects have not been completed compensated. The sample with the lowest conductivity and highest activation energy with a B concentration of ~$5x10^{17}$ cm^{-3} is close to *intrinsic*; in the context of an exact compensation of native defects by active boron acceptors. The two samples with B-atom concentrations of 1 and $2x10^{18}$ cm^{-3}, are p-type, and the activation energy is relative to the valence band edge. The dark conductivity varies by almost four orders of magnitude as the B-concentration increases from $5x10^{17}$ cm^{-3} to $2x10^{18}$ cm^{-3}. For the same changes in [B], the

photoconductivity varies by only a factor of 10. As noted above, and as shown in Fig. 3(a) the dark conductivity changes by about four orders of magnitude for this factor of four change in [B].

There are several factors that warrant additional discussion. The first relates to the deposition of B-compensated, near-intrinsic μc-Si. There are two factors that can play significant roles: i) the effective density of donor-like native defects; and ii) the ability to add relatively small and controlled amounts of B-atoms to the μc-Si film. LeComber et al. have estimated that the density of donor-like defects in their as-deposited, GD μc-Si films is ~2-4x10^{18} cm^{-3}. This is consistent with the observation that as-deposited dark conductivities in these films are about 2x10^{-2} S/cm. The Remote PECVD films had a lower as-deposited dark conductivity, ~6x10^{-4} S/cm, which is also consistent with the fact that a B-concentration of about 5x10^{17} cm^{-3} was required for *exact numerical compensation.* Since the conductivity ratios of these as-deposited films are greater than the ratio of the relative donor-like defect concentrations, we conclude that the relationships between the dark conductivity, and the defect-site and compensation doping densities are not simply determined by considerations of *exact numerical compensation.* We propose that the origin for these differences is in the inherently diphasic character of the μc-Si films; e.g., the internal interfaces between the crystalline and amroprhous constituents.

The second issue relates to the controlled incorporation of dopant atoms to compensate native donor-like defects. From the data in Fig. 3(b), this window is narrow. Our experience with deposition chamber histories indicates that if B-compensated intrinsic μc-Si layers are to be used in device structures, then they should be deposited in a dedicated chamber that is not used to deposit other more heavily doped p-type or n-type μc-Si layers, or Si,C alloy films. Unfortunately, we have only one chamber available for all of our amorphous Si and microcrystalline Si related studies.

The variation of the photoconductivity as a function of either the B-atom concentration, or the dark conductivity activation energy raises questions relative to the way the photoconductivity is to be interpreted. In the a-Si:H system, the photoconductivity shows a significant decrease as the dark conductivity transport mechanism changes from electron to hole dominated. This decrease is approximately three orders magnitude. In contrast, the photoconductivity in the μc-Si does not show a

similar drop as the material changes from electron-dominated dark conduction to hole-dominated dark conduction, i.e., from n-type to p-type. The magnitude of the dark conductivity, when normalized to the incident photon flux, and in particular to fraction of that radiation that is capable of producing hole-electron pairs, suggests that the photoconductive gain is high, and consistent with two carrier transport over the range of compositions studied. This is also consistent with the results of experiments on p-i-n structures that have been fabricated using the B-compensated μc-Si as the i-region material. These experiments have yielded relatively high short circuit current densities, ~5-10 mA/cm^2 to 0.5 AM1 radiation, indicating a significant two carrier current flow in the i-region material.

We have observed that the intrinsic μc-Si exhibits a high photoconductivity, but no *detectable* Staebler-Wronski effect. There are two possible explanations: i) the defect density in the B-compensated μc-Si is too high, in the sense that it masks any ability to detect light-induced defects; or ii) the recombination process that terminates the life-time of a photo-generated electron-hole pair does not occur in the amorphous regions between the crystallites. The relatively high photoconductivity over a doping range that includes a transition from n-type to p-type suggests that recombination may be dominated by centers at the interface between the crystalline and amorphous components of the μc-Si, or within the crystallites themselves. The kinetics of an interface dominated process would be influenced by the offsets at the respective band edges, as well as any band-bending that favors trapping of the holes. A similar argument could apply to hole-trapping within the crystallites; however, this is not likely due to the performance of the B-compensated material in p-i-n solar cells.

A.4. B-compensated μc-Si alloys by reactive magnetron sputtering

We have had considerable difficulty in reproducing results on B-compensated μc-Si by remote PECVD, primarily due to chamber cleanliness issues in our remote PECVD system. This prompted us to switch a portion of our effort on B-compensated μc-Si to the dual magnetron sputtering system. Reactive magnetron sputtering (RMS) is chemically cleaner than Remote PECVD when used to prepare μc-Si:B because the dopant is introduced in the solid phase rather than as a gas so that the problem of gas adsorption and release during subsequent depositions is eliminated. Three new targets were purchased, one 99.9999 purity undoped silicon, and two doped with boron to resistivities of 0.005-0.020 Ω-cm, and ~ 0.1 Ω-cm, respectively. These

experiments, to be discussed in more detail in another NREL sub-contract report, have shown that the variation of dark conductivity, and photoconducitivity, as a function of B-atom compensation of native defects, and B-doping, could be reproduced using B-atom incorportion via the RMS process. The behavior of the RMS films was qualitatively and quantitatively the same as in the remote PECVD films.

A.5. a-Si,C:H and μc-Si,C alloys

We have extended the remote PECVD process to the deposition of undoped and doped a-Si,C:H and μc-Si,C alloy films. This has been accomplished by adding the carbon atom source gas, CH_4, downstream, along with the Si and dopant atoms sources, and for the case of μc-Si,C, also downstream injection of H_2. We have compared the dark conductivities of the a-Si,C:H and μc-Si,C alloy films, respectively, with those of a-Si:H and μc-Si, and have been shown that the decreased conductivity of the Si,C alloy films can be attributed to the wider band-gaps of the Si,C alloys. For the case of the μc-Si,C films this means that the dark conductivities are also limited by thermal emission of carriers from the Si crystallites into the a-Si,C:H material that separates the Si crystallites (this is discussed in more detail later on in the report).

The conditions for depositing a-Si,C:H films are essentially the same as those used for device-quality a-Si:H films, except that the C-atom source gas CH_4 is introduced downstream along with the Si-atom source gas SiH_4, and the combined flow of the SiH_4+CH_4 mixture is maintained at a level comparable to the flow of SiH_4 for the a-Si:H depositions. We define the SiH_4 fraction of these gas mixtures as X = SiH_4/(SiH_4+CH_4), and have varied X between 1.0 and 0.33, to deposit a-Si,C:H films that contain up to ~15 at.% C. For the deposition of the μc-Si,C:H alloy films, a flow of 30 sccm of molecular hydrogen, H_2, was added downstream to the SiH_4/CH_4 source gas mixture. For the deposition of doped a-Si,C:H or μc-Si,C:H, the dopant-atom source gases, diborane, B_2H_6, and phosphine, PH_3, were premixed with the Si- and C-atom source gases and also injected down-stream.

A series of a-Si,C:H alloy films with different C-atom concentrations has been deposited by varying X between 1 and 0.33. The local bonding in these films was characterized by IR absorption. These IR features include bond-stretching and bending absorptions due to Si-C, CH_3 and C-SiH groups. Each of these spectral features increases in strength as the CH_4 fraction in the source gas mixture is

increased, i.e., as X decreases from 1.0 to 0.33.

We have also studied the electrical and optical properties of this same series of a-Si,C:H alloy films. The dark conductivity, the photo-conductivity and the effective optical bandgap are essentially the same as those in a-Si,C:H alloy films deposited by the GD method using approximately the same SiH_4/CH_4 source gas mixtures. The bandgap and photoconductivity data indicate that as X decreases from 1 (a-Si:H) to 0.5, the E_{04} bandgap increases from ~1.90 eV to ~2.25 eV, and the photoconductivity for illumination by white light at ~50 mW/cm^2, decreases from $5.5x10^{-5}$ S/cm to $8.9x10^{-9}$ S/cm, both effects similar to the results reported for GD films. E_{04} is 2.05 eV for the undoped X = 0.67 a-Si,C:H.

p-type and n-type a-Si,C:H alloy films have also been deposited by adding the dopant atom gases to the downstream injected SiH_4/CH_4 gas mixture. The most extensive of these studies have been confined to a single SiH_4/CH_4 source gas mixture, X = 0.67. For the highest diborane doping gas ratio used, (1%), and for X = 0.67, the conductivity of the p-type a-Si,C:H was $1.4x10^{-6}$ S/cm with an activation energy of 0.46 eV. This conductivity is about a factor of 500 less than what is obtained in a-Si:H for the same doping gas fraction. The decreased dark conductivity is consistent with an increased activation energy: 0.46 eV in a-Si,C:H, and 0.31 eV in a-Si:H. For the highest phosphine doping gas ratio, also (1%), the dark conductivity was $3.5x10^{-5}$ S/cm with activation energy of 0.41 eV. This is about a factor of 570 less than that of a-Si:H grown from the same relative concentration of PH_3. The decreased conductivity is also in accord with an increased activation energy: 0.41 eV as compared to 0.25 eV. This means that the smaller conductivities for the doped a-Si,C:H as compared to a-Si:H result mostly from the larger activation energies, but that the conductivity prefactors, which characterize transport in extended states of the conduction and valence bands of a-Si,C:H, are essentially the same as in a-Si:H.

μc-Si,C:H alloy films have been deposited by RPECVD by adding H_2 to the downstream injected SiH_4/CH_4 source gas mixtures. The combined effective flow rate of the SiH_4/CH_4 mixture was maintained 1~2 sccm, and the flow rate of the H_2 was fixed at 30 sccm, the same ratio as used for the deposition of the μc-Si films with the highest fraction of crystallinity. The degree of crystallinity in the μc-Si,C:H alloy films has been investigated by Raman spectroscopy and transmission electron microscopy (TEM). Studies by TEM imaging and Raman scattering indicate a decreased amount

of crystallinity in μc-Si,C:H as compared to μc-Si prepared under similar deposition conditions. Raman spectra for μc-Si,C:H show that μc-Si,C:H alloy films exhibit a sharp feature at 520 cm^{-1} that is the same as the sharp crystalline feature found in μc-Si films. This establishes that at least one of the possible crystalline components in these films is Si. The fraction of crystallinity can be estimated from the ratio of the Raman scattering in the crystalline "TO" feature to that in the 470 cm^{-1} "TO" band; this is ~10-20%. We have obtained the Raman spectrum over a spectral range from about 100 to 1500 cm^{-1}, and have found no evidence for spectral features associated with crystalline SiC, or with either of the crystalline forms of carbon: diamond or graphite. This means that the C-atoms incorporated into the μc-Si,C:H alloys must then be included in the amorphous material that is interposed between the Si crystallites. This interpretation of the Raman and TEM data is supported by the IR spectra. By adding additional CH_4 into the source gas mixtures that include H_2, the degree of crystallinity of deposited alloy films decreases. Hydrogenated amorphous carbon films have been deposited under the same deposition conditions, but with no SiH_4 in the source gas mixture, and with the flow rate of H_2 maintained at 30 sccm.

Deposition of heavily doped, p-type and n-type μc-Si,C:H alloy films also has been accomplished by remote PECVD, however for a limited set of gas flow conditions. The dopant atom source gas, either diborane or phosphine, was added to the Si- and C-atom source gas mixture at concentrations of 0.1% and 1%, and for X = 0.33, 0.5 and 0.67. Films deposited with 1% *gas phase doping* of the X = 0.67 Si-atom and C-atom source gas mixture were amorphous as determined by analysis of the Raman scattering. Films deposited from 0.1% doping gas mixtures were microcrystalline for X = 0.67 and 0.50, but became amorphous when the silane fraction was further reduced to 0.33. Raman scattering was also the characterization technique used to distinguish between the amorphous and microcrystalline character of these less heavily doped films. We have also studied the properties of undoped Si,C alloy films grown under flow conditions which included 30 sccm of H_2. μc-Si,C:H films were obtained for X = 0.67 and 0.50, but not for X = 0.33. It is interesting, and important to note that the doped and undoped a-Si,C:H alloys that are produced with H_2 dilution of the SiH_4/CH_4 mixtures have properties which are generally different from a-Si,C:H films produced without the H_2 flow. For example, the conductivity of p-type a-Si,C:H films deposited with a gas phase doping fraction of 1.0% differ by a factor of 10, with the film grown without H_2 dilution having the higher conductivity and lower activation energy. This is consistent with the fact that hydrogen atoms can,

under certain circumstances combine with dopant atoms to produce local bonding configurations that reduce the doping efficiency of the B- and P-atoms. However, as noted above, the dark conductivities of p-type a-Si:H films, deposited with, and without H_2 dilution were essentially the same.

A.6. a-Si:H,O and a-Si:H,N Alloys

We have established deposition process procedures for the formation of alloys of Si,O,H and Si,N,H with variable concentrations of O and N respectively. Using O_2 and N_2 as the source gases, we find that a higher incorporation of bonded O, relative to bonded N, for the same gas phase ratios of O_2 and N_2 flow relative to silane flow. This is anticipated based on differences in the effectiveness in generating active oxygen and nitrogen precursors.

A.6.1. a-Si:H,O Alloys

We have used the frequency of the Si-O stretching vibration to monitor the film composition, and have found that the relative oxygen concentration (x in the alloy SiO_x) is approximately linear in O_2 gas flow. For x between 0 and 1, there is a relatively slow increase in the band-gap, whereas for x>1 the gap increases more rapidly (our results agree with H. Philipp). For sub-oxides with E_{04} band-gaps less than about 1.85 eV, the dark conductivity activation energy is less than $E_g/2$, whereas for band-gaps greater than 1.85 eV, it is larger than $E_g/2$. For x between 0.0 and 0.7, the photoconductivy drops by about a factor of two, whereas it drops by more than three orders of magnitude between x = 0.7 and x = 1.1. The phototransport properties of these alloys films will receive further study, primarily as candidate materials for the i-regions of the wide band-gap cell of triple tandem PV devices.

A.6.2. a-Si:H,N alloys

We have studied the properties a-Si:H:N alloys over a N-alloy range in which the E_{04} band-gap shifts from 1.9 eV for a-Si:H, to approximately 2.4 eV. We have studied: i) the photoconductive response at high light-levels, the decay of the photoconductivity under 100 mW-cm^{-2} illumination, and the IR transmission as a function of the silane to molecular N_2 flow rates. Film thicknesses for this study were in the range of 0.3 to 1.0 μm, and were determined by combinations of cross-sectional

TEM imaging, and optical spectroscopy, i.e., analysis of interference fringes in the transparent region below the absorption edge. The ratio of photoconductivity to dark conductivity did not change in any significant way with the addition of N to the a-Si:H films, and is typically of the order of $3\text{-}5\text{x}10^4$. This supports our previously reported results. Films were light-soaked for periods of time up to about 90 hours. In general the decrease of the photoconductivity reached its steady-state value for 1000 minutes of light-soaking. The ratio of the initial photoconductivity to the steady-state, light-soaked photoconductivity was typically between 10 and 15. Photodegradation curves were analyzed in terms of a stretched exponential. We have previously shown that the time constant for this function can be determined by fitting the decay curve to a power law function, and finding the time at which the derivative of that fitted function goes through its maximum value. Analysis of the photodegradation by this technique yields characteristic times of the order of 3 to 5 minutes. The corresponding values of the light to dark ratio of currents, the ratio of initial to steady-state, light-soaked photoconductivities and degradation times are: 7×10^4, 15, and 6 minutes, respectively, so that the addition of bonded N-atoms does not change the properties of these alloys with respect to a-Si:H, to the same degree that the addition of C-atom concentrations that change the E_{04} band-gap by a similar amounts.

A.7. deposition of a-Si,Ge:H alloys by Remote PECVD

We have established that a-Si,Ge:H alloy films can be deposited by Remote PECVD by remotely exciting He, and injecting SiH_4/GeH_4 mixtures down-stream. Our initial results indicate that the amount of Si polyhydride in a film deposited at a given T_S is increased over what has been previously found in films deposited from pure SiH_4. This indicates that gas phase reactions have occurred between the down-stream activated SiH_4 and GeH_4 species. These reactions have produced a precursor which favors the Si polyhydride deposition reactions. Using our model for film deposition, as discussed above, and our previous observations relative to Ge suppression of Si polyhydride groups in RMS, films, we conclude that i) gas phase precursor formation has occurred and 2) that Si polyhydride groups are being introduced into the film via physical processes, as well as surface chemical reactions.

B. Transport and Optical Properties of a-Si and μc-Si Films

B.1. Barrier limited transport in μc-Si and μc-Si,C alloys

The dark conductivity data for the remote PECVD microcrystalline films is summarized in Table III. This table also includes conductivity data for a-Si:H and a-Si,C:H films. The conductivity, σ, deduced from these data, display a temperature-activated behavior characteristic of semiconductors:

$$\sigma = \sigma_0^* \exp (- E_\sigma^* / kT). \quad (1)$$

σ_0^* is the conductivity prefactor, and E_σ^* is an effective activation energy. There is no *simple* interpretation for E_σ^* for an amorphous semiconductor in which the motion of the Fermi level through the gap is determined by the density of defect states within the gap. However, *differences* between values of E_σ^* for different doping and/or alloy composition can be proportional to the energy differences between the edges of the transport bands, and the Fermi level position as *extrapolated* to T = 0K. The conductivity, $\sigma(T)$, for an n-type film at any temperature, T, can always be written as:

$$\sigma(T) = \sigma_0 \exp \{ (E_C(T) - E_F(T)) / kT \}, \quad (2)$$

where σ_0 is a conductivity characteristic of transport in the extended states, ~ 2000 S/cm for a-Si:H, and about an order of magnitude higher than the values of 150 to 200 S/cm previously proposed. $E_C(T) - E_F(T)$ is the *actual* difference in energy

Table IV. Character of Films Produced by Remote PECVD

SiH_4 / (SiH_4+CH_4)	Doping Gas Ratio	Hydrogen Flow (sccm)	Amorphous or Microcrystalline
1.0	0	0	amorphous
1.0	to $1x10^{-2}$ B_2H_6	0	amorphous
1.0	to $1x10^{-2}$ PH_3	0	amorphous
1.0	0	30	microcrystalline
1.0	to $1x10^{-3}$ B_2H_6	30	microcrystalline
1.0	> $1x10^{-3}$ B_2H_6	30	amorphous
1.0	to $1x10^{-2}$ PH_3	30	microcrystalline
1.0	> $1x10^{-2}$ PH_3	30	amorphous
0.67	all doping levels to 10^{-2} PH_3 & B_2H_6	0	amorphous
0.33 & 0.50	0	30	amorphous
0.67	0	30	microcrystalline
0.67	< $1x10^{-2}$ B_2H_6	30	microcrystalline
0.67	$1x10^{-2}$ B_2H_6	30	amorphous
0.67	< $1x10^{-2}$ PH_3	30	microcrystalline
0.67	$1x10^{-2}$ PH_3	30	amorphous

between the transport band, i.e., the conduction band, and the Fermi level at the temperature T. This energy difference is given by:

$$E_C(T) - E_F(T) = E_{\sigma}^* - (\gamma_C - \gamma_F)T, \quad (3)$$

where γ_C is the shift of the conduction band edge with temperature, T, determined from the shift of the optical gap with T, and γ_F is the temperature shift of the Fermi level. For a-Si:H, a-Si,C:H, μc-Si and μc-Si,C alloys, the behavior of the conductivity prefactor, σ_0^*, with doping is qualitatively different from what is generally observed in doped crystalline semiconductors. This is behavior illustrated in Fig. 4, which displays a plot

of σ_0^* versus E_σ^* for all of the Si,C alloy samples listed in Table IV, both amorphous and crystalline, and for the most heavily doped μc-Si samples. These data display what has been designated a Meyer-Neldel behavior, which is characteristic of amorphous semiconducting materials, including a-Si based alloys, and embodied in the following relationship,

$$\sigma_0^* = C \exp(E_\sigma^*/E_0). \quad (4)$$

The Meyer-Neldel fit parameters, C and E_0 in Eqn. (4), are different for the two groups of films; i) the a-Si,C:H and μc-Si,C alloys, and ii) the heavily doped μc-Si. The data for all of the Si,C alloy samples have activation energies $E_\sigma^* > 0.18$ eV, and display a linear dependence with $C \approx 2.5 \pm 1$ S/cm and $E_0 = 0.12 \pm 0.02$ eV. In contrast, the data for most heavily doped μc-Si films, with activation energies, $E_\sigma^* < 0.1$ eV, also display a linear behavior, but with very different constants:

Table IV. Electrical Properties of Films grown by Remote PECVD

Material	H_2/SiH_4 Ratio	Dopant Gas Fraction	Dark Conductivity 300K (S/cm)=$(\Omega\text{-cm})^{-1}$	Activation Energy (eV)
a-Si:H	0	0	2.4×10^{-10}	0.80
a-Si:H(n)	0	1×10^{-2}	2.0×10^{-3}	0.25
a-Si:H(p)	0	1×10^{-3}	4.0×10^{-7}	0.59
a-Si:H(p)	0	1×10^{-1}	2.4×10^{-3}	0.31
μc-Si	30:1	0	6.0×10^{-4}	0.30
μc-Si(n)	30:1	3×10^{-5}	0.2	0.08
μc-Si(n)	30:1	3×10^{-4}	5.0	0.05
μc-Si(n)	30:1	1×10^{-2}	50-100	0.02
μc-Si(p)	30:1	1×10^{-5}	6.0×10^{-8}	0.66
μc-Si(p)	30:1	2×10^{-4}	7.0×10^{-4}	0.24
μc-Si(p)	30:1	1×10^{-3}	6-10	0.04
a-Si:H(p)	30:1	1×10^{-2}	4.0×10^{-5}	0.40
a-Si:H(p)	30:1	1×10^{-1}	3.0×10^{-3}	0.30
a-Si,C:H	0	0	2.3×10^{-13}	0.99
a-Si,C:H(n)	0	1×10^{-2}	3.5×10^{-5}	0.41
a-Si,C:H(p)	0	1×10^{-3}	2.0×10^{-9}	0.69
a-Si,C:H(p)	0	1×10^{-2}	1.4×10^{-6}	0.46
μc-Si,C(n)	30:1	3×10^{-4}	5.0×10^{-4}	0.35
a-Si,C(n)	30:1	1×10^{-2}	1.3×10^{-3}	0.23
μc-Si,C(p)	30:1	1×10^{-3}	6.3×10^{-4}	0.18
a-Si,C:H(p)	30:1	1×10^{-2}	1.4×10^{-7}	0.56

$C \approx 305 \pm 10$ S/cm and $E_0 \approx -0.02 \pm 0.005$ eV. E_0 is positive for the Si,C alloy films, but negative, and also smaller by a factor of 5 for the heavily doped μc-Si films. The a-Si:H, and lightly doped μc-Si films, with $E_\sigma^* > 0.2$ eV display a behavior that is essentially the same as that of the Si,C alloy films. Using the relationships presented in Eqns. (1) - (4), we can write the following expression for the conductivity prefactor, σ_0^*, in the experimental fit to the conductivity:

$$\sigma_0^* = \sigma_0 \exp \{ (\gamma_C - \gamma_F) / k \}. \quad (5)$$

The data that we have included in Fig. 4, are for n-type and p-type doped films, as well as undoped films; the same is true for the data presented in Figs. 5 and 6. Figure 5 is a plot of the room temperature conductivity, σ_{rt}, as a function of the activation energy, E_σ^*, for all of the Si and Si,C alloy films contained in Table IV. These data can each be fit with an exponential function;

$$\sigma_{rt} = \sigma_{rt}^* \exp (-E_\sigma^*/kT_{eff}). \quad (6)$$

The two fits are differentiated by different values of σ_{rt}^*, and T_{eff}. For the Si and Si,C films with $E_\sigma^* > 0.2$ eV, $\sigma_{rt}^* \sim 3 \pm 1$ S/cm, and $T_{eff} = 390$K, whereas for the four heavily doped μc-Si films with $E_\sigma^* < 0.1$ eV (these are the same four μc-Si films used in the Meyer-Neldel plot in Fig. 2), $\sigma_{rt}^* \sim 300 \pm 50$ S/cm and $T_{eff} \approx 125$K. Note that the values of C from the Meyer-Neldel fits and σ_{rt}^* from the corresponding fits in Fig. 5 are essentially the same. The second branch of the Meyer-Neldel plot was predicted by Beyer and Overhof, and is not directly accessible in single-phase heavily doped a-Si:H because the Fermi level can not be moved into the band-tail states; however, these states are accessible by tunneling in microcrystalline maerials.

It can be shown that the values of T_{eff} from the two fits to the data in Fig. 5 are consistent with the two different E_0 constants determined from the Meyer-Neldel fits. This is confirmed by: i) comparing Eqns. (1) and (6); ii) equating C and σ_{rt}^*, and then iii) extracting a relationship between T_{eff} and E_0:

$$kT_{eff} = (E_0 \, kT_{rt}) / (E_0 - kT_{rt}). \quad (7)$$

T_{rt} is taken as 300K, the approximate temperature at which the *room temperature* data were obtained. As noted above, the conductivity data for a-Si:H, and for lightly doped μc-Si with $E_\sigma^* > 0.18$ eV display a Meyer-Neldel behavior with essentially the same constants as the data for the Si,C alloys with $E_\sigma^* > 0.1$ eV.

Table V. Band Offsets for μc-Si and μc-Si,C

Band offset	Conduction Band E_C(amorphous) - E_C(crystal)	Valence Band E_V(amorphous)- E_V(crystal)
Material	**(±0.05 eV)**	**(±0.05 eV)**
a-Si to c-Si	+ 0.30 eV	+ 0.30 eV
a-Si,C:H to c-Si	+ 0.50 eV	+ 0.50 eV
Difference in Offsets	+ 0.20 eV	+ 0.20 eV
Experimental Data (Fig. 3)-Average value:+0.20±0.03 eV		

Another significant aspect of the conductivity data in illustrated in Fig. 6, where we have plotted activation energies for a-Si,C:H and μc-Si,C, E_σ^*(Si,C), as a function of the *corresponding* activation energies for a-Si:H and μc-Si, E_σ^*(Si), for films that have been deposited using the same relative ratios of dopant gas to the Si-atom, or Si-atom plus C-atom source gas mixtures. These data, included in Table V, display the following linear relationship:

$$E_\sigma^*(Si,C) = \delta E_\sigma^*(0) + a\, E_\sigma^*(Si) \qquad (8)$$

where δE_σ^* = 0.20±0.03 eV and a = 0.92±0.05. As we have noted above by comparing Eqns. (1) and (2), the values of E_σ^*(Si) and E_σ^*(Si), have an interpretation in terms of a band picture that can apply by extrapolation to T = 0 K; e.g., for n-type materials,

$$\Delta E_\sigma^* = E_\sigma^*(Si,C) - E_\sigma^*(Si) \approx (E_C - E_F) \text{ for } T \to 0. \qquad (9)$$

This means that the experimentally determined relationship in Fig. 3 applies to band picture at T = 0K, rather than to a band picture at the measurement temperature. The other band offset values in Table III are derived from the band model described below. It must also be noted that the relationship in Eqn. (9) is contingent on another aspect of carrier transport in the Si and Si,C alloy materials. Beyer and Overhof have pointed out that the Fermi level position at any temperature, $E_F(T)$, can be determined from the conductivity data by assuming an appropriate value for σ_0; i.e.,

$$| E_t - E_F(T) | = kT \ln[\sigma_0/\sigma(T)] \qquad (10)$$

where E_t is the energy of the transport band, e.g., E_V or E_C, the band edges defined by the mobility gap. A necessary condition for the relationship in Eqn. (9) to hold is then

that the same values of σ_o apply for both the Si and the Si,C alloy materials. We have used Eqn. (10) to calculate $|E_t - E_F(T)|$ for T = 300K for the same set of Si and Si,C films that have been used for the plot in Fig. 6. The average value of $|E_t - E_F(300K)|$ for the Si,C films is greater than the average value of $|E_t - E_F(300K)|$ for Si by ~0.19 eV, and is thus approximately equal to the intercept of 0.20 eV for the plot in Fig. 6. This conclusion is independent of the particular value used for σ_o.

One of our research objectives has been to understand the different transport limitations in μc-Si and μc-Si,C alloys in terms of their microstructures. To this end, three aspects of the experimental data have been combined in a model for the carrier transport i) the microstructure, including the chemical nature of the crystalline and amorphous components; ii) the Meyer-Neldel plots in Fig. 5 for all of the Si and Si,C materials with $E_\sigma^* > 0.18$ eV, and for μc-Si with $E_\sigma^* < 0.1$ eV; and iii) the linear relationship between E_σ^*(Si,C) and E_σ^*(Si) in Fig. 3.

There has been extensive modeling of carrier transport in two phase materials. For μc-Si and μc-Si,C, the crystalline component is Si, and the amorphous component, a-Si:H or a-Si,C:H. If ρ(1) as the resistivity of the crystalline component and ρ(2) is the resistivity of the amorphous component, then the data in Table IV indicate that for all gas phase doping ratios, ρ(2) » ρ(1). This assumes that the crystalline and amorphous constituents contain the about the same concentrations of dopant atoms, so that the dark conductivity of the crystalline Si phase is then significantly higher than either of the respective amorphous phases. These differences in conductivity between the doped Si crystallites and the amorphous materials can be brought about by differences in either the free carrier concentrations and/or the carrier mobilities. Since the bandgap of the Si crystallites, ~ 1.1. eV, is smaller than the bandgap of the a-Si:H, ~ 1.7 eV, or a-Si,C:H, ~ 2.1 eV, this means that we can treat the microcrystalline materials as arrays of back-to-back Schottky barriers in which the doped crystalline Si constituents are *pseudo-metals*, or free-carrier reservoirs, and the doped amorphous regions are the *more resistive semiconductor regions*. For the n-type materials, these barriers are better described as n^+/n^- heterojunctions. The potential configuration for these heterojunctions are equivalent to a Schottky barrier, provided that the conduction band offset is positive, e.g., for n-type material, E_c(a-Si:H) - E_c(c-Si) > 0. We will later present experimental evidence, and theoretical justifications for this conduction band alignment. Assume, that this type of band alignment exists, the resistivity of the diphasic microcrystalline material, ρ*, can be

approximated by the following relationship:

$$\rho^* \approx \{n(1)\, q\, \mu_b\}^{-1}, \qquad (11)$$

where n(1) is the free-carrier concentration in the crystalline material, and μ_b is an *effective mobility* for the transport of free carriers from the crystalline material through the amorphous regions. If thermionic emission *over* interfacial barriers limits the current, then the effective mobility in Eqn. (11) is thermally-activated and given by,

$$\mu_b = \mu_o \exp(-E_b/kT), \qquad (12)$$

where μ_o is a band mobility in the amorphous material, and E_b is the barrier height at the crystalline/amorphous interface. If transport between the two phases is by thermally-assisted tunneling, then a similar expression for the mobility will hold; E_b will be much smaller than for the thermionic emission case, and the physical interpretation of E_b will also require modification. For thermionic emission case, E_b has two contributions; i) one from the band offset between the conduction or valence band edges of the crystalline and amorphous components, and ii) the second from the relative positions of the Fermi levels in the crystalline and amorphous components, i.e., from band-bending at this internal interface. This interpretation for the exponential behavior of μ_b as in Eqn. (12) is not unique. For example, one can associate the exponential dependence of the dark conductivity in diphasic materials with an *effective* carrier concentration, rather than an activated mobility. For this case;

$$n = n(1)\exp(-E_b/kT) \qquad (13)$$

n is the density of carriers that are thermally excited over the interfacial barrier, and n(1) is the free carrier density in the crystalline phase.

To specify a particular mechanism for carrier transport across the internal crystalline-amorphous interfaces, it is first necessary to develop a model for the band-alignment at the conduction and valence band edges of the two constituent phases. We start with the band diagram in Fig. 7(a) for intrinsic μc-Si. This alignment between the Si crystallites, and the amorphous encapsulant has been determined in the following way: i) since the elemental constituents of both phases are Si, we assume that the respective mid-bandgap levels (*not* the Fermi levels) in a-Si and c-Si line-up (this is equivalent to saying that the average separation between the bonding and anti-bonding states depends on bond chemistry, but is insensitive to the degree of long range order); ii) we assume an effective gap for the crystalline Si component of ~1.1 eV; iii) we use optical data to define an effective mobility bandgap for a-Si:H at ~1.7 eV; and finally iv) we use the doping data of LeComber and Spear to define the spread of band-tail states into the gap of the a-Si:H. For the μc-Si,C band alignment

diagram in Fig. 7(b), we assume: i) that mid-gap alignment is maintained in spite of the small (~10-20 at. %) incorporation of C-atoms in the amorphous phase; ii) an effective bandgap of ~ 2.1 eV for a-Si,C:H, consistent with optical data for our samples; and iii) that band-tailing into the gap is approximately 33% greater in a-Si,C:H than in a-Si:H. This assumes that the dominant contribution of the band-tailing comes from compositional disorder, and that alloy disorder is smaller, but none-the less present. Finally, we assume equal offsets at the respective valence and conduction band edges. These assumptions fix the conduction and valence band offset energies at the values presented in Table V. The difference between these energies for the Si and Si,C alloy materials (with 2.1 eV bandgaps) is 0.20 eV, and is approximately equal to the energy intercept of 0.20±0.03 eV for the fit to the conductivity activation energy data in Fig. 6, which includes both n-type and p-type materials. This correspondence means that the Fermi level positions, in the limit of T = 0K, in similarly doped a-Si:H and a-Si,C:H are displaced relative to each other by approximately the conduction and valence band offset energies. This also means that for a given gas phase doping, the Fermi level shift relative to the middle of the gap is the same for a-Si:H and a-Si,C:H. This is also consistent with the interpretation of the Meyer-Neldel relationships shown in Fig. 2 [6,7]; e.g., the Meyer-Neldel rule derives from a statistical shift of the Fermi level through the distribution of states in the pseudo-gap. A common rule for a-Si:H, a-Si,C:H and μc-Si (E_σ^* >0.2 eV), and for μc-Si,C can then be interpreted as demonstrating that *relative to the center of the pseudo-gap*, the densities of defect states in a-Si:H and a-Si,C:H are essentially the same.

Figures 7(c) and 7(d) indicate the interfacial alignment of the conduction bands for light and degenerate doping in μc-Si and μc-Si,C, respectively. Following the data Tables II and III, the Fermi level in the crystalline component, c-Si, never lines up within the distribution of band-tail states in the a-Si,C:H component so that direct tunneling into these states does not occur. The reason for this is related to the limited extent which the Fermi level can move through the defect states of the a-Si,C:H material. For transport between the c-Si and a-Si,C:H to involve tunneling into the band-tail states of the a-Si,C:H, the carrier source must be no more than a few kT below the extended states of the a-Si,C:H. These conditions for tunneling are not met in μc-Si,C, so that thermionic emission over the internal barrier limits the carrier transport. All of the measured activation energies in the Si,C materials are consistent with this picture: they are ≥ 0.18 eV, and therefore > 7 kT at room (see Fig. 8). The conductivity measurements were made at low fields, ~200 V/cm, where the I-V

characteristics are linear. This is consistent with a barrier limited ohmic transport process since the average potential drops across the barrier, and over the entire extent of the amorphous region are significantly smaller than kT for these relatively small fields. Average fields > 10^4 V-cm^{-1} are required to drive the I-V characteristics into a non-ohmic behavior.

The transport in the Si-materials is qualitatively different than in the Si,C alloys. Consider first the a-Si:H and μc-Si films with activation energies > 0.2 eV. These materials display essentially the same behaviors in Figs. 4 and 5, as the Si,C alloys. This is interpreted to mean that thermionic emission over interfacial barriers applies. However, the fit parameters to the second exponential region in the conductivity plot in Fig. 2 for activation energies < 0.1 eV are markedly different than the fit parameters for activation energies greater than 0.2 eV. Analyses of the these data indicate that thermally-assisted field-emission into the band tail states of a-Si:H from the c-Si component is the dominant transport process in these heavily doped μc-Si materials (Fig. 7(c) and Fig. 8).

B.2. Minority Carrier Transport in a-Si and μc-Si

We have used the steady state photocarrier grating technique (SSPG) to study minority carrier transport in a-Si:H and μc-Si. To test our apparatus, we used a previously measured sample by supplied by Dr. W. Paul of Harvard. His group obtained a value of 1356±100Å for the ambipolar diffusion length, L, using an illumination level, I = 1 mW of laser power. We obtained a value of L = 1150±100 Å at a power level of 4 mW. L was found to exponentially decrease as the laser intensity increased, and using our data, we have found that $L = 1368.6 * e^{-0.045*I}$. For an illumination of 1 mW power, this yields L = 1308±100 Å, a value close to that determined by Professor Paul's group. We also studied B-compensated μc-Si, μc-Si:B, prepared by Remote PECVD using 10 sccm of 10 % silane in helium, and 10 sccm of 1ppm diborane in helium. At an illumination of level 10 mW, and under the application of 100 volts, the μc-Si:B photoconductivity is ~ 10^{-2} $(\Omega\text{-cm})^{-1}$. For the same illumination and an electric field of E = 243 volt-cm^{-1}, and assuming zero surface recombination velocity, we have obtained L = 403 ± 50 Å. If we assume a similar dependence between L and I as for a-Si:H, this corresponds to a value of L ≈ 600 Å for I ≈ 1 mW.

We have also used this technique to evaluate minority carrier transport in a-Si,N:H alloys. For alloys with band gaps between about 1.9 and 2.1 eV, we find values of L ~ 500-600 Å. This result coupled with measurements of the photoconductivity and Stabler-Wronski effect make these alloys interesting candidates for i-layer materials in tandem solar cells.

B.3. Transport and Defect States by Femto-Second Spectroscopies

We have collaborated with Professor Heinz Kurz's group at RWTH in Aachen, Germany, and have studied the properties of a-Si:H on a Femto-second time scale. In one set of experiments, we have studied the spectral- and time-resolved reflectivity and transmission of hydrogenated amorphous silicon, a-Si:H, with 50 fs time resolution. Electron-hole pairs are photo-excited into the extended states of a-Si:H by an ultrashort pump pulse at a photon energy of 2 eV. The spectral dependence of the optical response has analyzed in terms of a hopping model for the transport of the photogenerated carriers in the extended states of a-Si:H, and a hopping distance of 2.3 Å has been obtained.

In a second set of experiments, the temporal evolution of the photo-induced optical response is studied for a broad range of excitation densities from 10^{18} up to 10^{20} cm^{-3}, and on a time scale of up to 200 picoseconds, ps. The optical response has been analyzed in terms of recombination and trapping mechanisms for carriers in the extended states of a-Si:H. Non-radiative quadratic recombination has been identified as the dominant relaxation mechanism for photo-induced carriers in the extended states of photovoltaic grade a-Si:H with mid-gap defect state densities of the order of, or less than about 10^{16} cm^{-3}. For photo-generated carrier densities between 10^{18} cm^{-3} and 10^{20} cm^{-3}, and for time delays up to 200 ps, the experimental data do not show any indication for trapping of photo-excited free carriers into localized bandtail states, consistent with recent time-of-flight transport measurements .

B.4. Photoluminescence and PDS in μc-Si:B (Collaboration with University of Utah)

The photoluminescence, PL, spectra of samples of μc-Si:B, prepared by remote PECVD, were studied (at 4K and 77K) in a collaborative effort with Professor P.C. Taylor's group at the University of Utah. The films for these studies had different

amounts of B-incorporation, and covered a B-concentration range that corresponded to: i) n-type materials in which the active B-atom concentration was too small to compensate donor-like native bonding defects; ii) *quasi*-intrinsic μc-Si:B in which, the active B-atom concentration compensated the native bonding defects; and iii) p-type material in which the active B-concentration exceeded the density of native bonding defects.

For heavily doped μc-Si (both n-type and p-type) with high conductivities, ~ 6 S/cm for p-type and 40 S/cm for n-type, the photoluminescence is weak, and the PDS spectra indicates a relatively high density of mid-gap defect states characterized by sub-bandgap absorption constants in excess of 2-300 cm-1 at ~0.8 eV. These results are essentially the same as those obtained for doped a-Si:H. For B-compensated samples with low dark conductivities, ~10^{-7} to 10^{-5} S/cm, there are two strong PL features: i) at 0.8 to 0.9 eV and associated with band-tail to defect state transitions; and ii) at ~1.2-1.3 eV and associated with band-tail to band-tail transitions. These samples display sub-bandgap absorption constants below about 100 cm^{-1}, so that there is a correlation be stronger PL and lower sub-banbgap absorption.

C. Device Applications

C.1. Formation of a-Si and μc-Si TFT's

We have developed a process to form TFT devices by Remote PECVD. The process consists of three depositions done in sequence in the same deposition chamber, and post-deposition-lithography, etching and metallization to define the devices. We have formed TFT's by the sequential deposition of Si_3N_4, intrinsic a-Si:H, and n-doped a-Si:H by Remote PECVD. We have evaluated the electronic performance and have found electronic characteristics that are similar to state of the art TFT's formed by the GD process; e.g., channel mobilities of about 0.75 cm^2/V-s, and threshold voltages of about 2.5 V. We have have also fabricated devices with better TFT performance through i) the use of two-compent dielectrics, ii) processing the back of the channel region; and iii) by substituting μc-Si for the a-Si:H in both source and drain contacts, and the channel regions of the devices.

We have used inverted structures with a two-component dielectric layer: an stoichiometric SiO_2, prepared by remote PECVD and in contact with the metal

electrode (deposited onto the glass substrate), and a silicon nitride film, onto which the a-Si and/or μc-Si layers are deposited. The performance of MIS devices structures is critically dependent on the nitride material. Remote PECVD nitrides typically have both N-H and Si-H bonding, so that the demarcation point between hydrogenated *quasi-stoichiometric* nitrides and sub-nitrides (SiN_x, x<4/3) cannot be established by the bonded-H alone. We have varied the ratio of the N-atom to Si-atom sources gases, NH_3 and SiH_4, and deposited films that span a concentration range from hydrogenated sub-nitrides to nitrides.

TFTs, have integrated oxide/nitride dielectrics into an inverted gate structure in which the oxide is in contact with the W-gate, and the nitride is contact with the undoped a-Si:H channel. n^+ a-Si:H has been used for the source and drain contacts. The oxide, nitride, undoped a-Si:H, and n^+ a-Si:H layers are deposited sequentially by remote PECVD at 250°C, and the device structure is then defined by lithographic techniques. The deposition variables have been adjusted to yield stoichiometric SiO_2 layers with bonded-H below the level of IR detection. We have systematically varied the source gas ratio, R = NH_3 to SiH_4, between 2.5 and 12.5. Using on-line AES, Si-Si bonds are present for R less than 9, but not for source gas ratios of 10 or more The electrical characteristics of the TFT's improve significantly as the gas phase ratio R is increased from 2.5 to approximately 10, and then decrease as R is further increased to 12.5. Additional improvements in the electrical performance of the TFTs have been made by i) a pre-deposition nitridation of the a-Si:H surface for the bottom-gate devices, and ii) a post-deposition processing of the back-side of the channel for the top-gate structures that is performed after the patterning. The back surface nitridation of the channel reduces carrier scattering and/or recombination processes at that surface, and increases the channel mobility. The performance of the TFTs peak for a source gas ratio of ~10, where the channel mobility is ~1.6 cm^2/V-s, the threshold voltage is 2.3 V; and the ratio of I_{on} to I_{off} is in excess of 10^5. Further improvements in performance have been realized by using doped μc-Si source and drain contacts, and by using B-compensated μc-Si material for the channel region. For, example, channel mobilities of ~2.4 cm^2/V-s have been obtained in TFTs with μc-Si source, drain and channel regions.

C.2. PV device structures

We have formed p-i-n junctions that are fabricated using only μc-Si. These p-i-n

structures have the following layer dimensions: the p-layer, and n-layers are 300Å thick and the i-layer is 2800Å thick. The i-layer is grown from the boron-compensated material discussed above, The p-i-n diodes exhibit i) rectification ratios of about 10^4 at a 0.5 V bias level and have ii) short circuit current densities of about 4 mA/cm^2, and open circuit voltages of 0.4 V. These structures are "non-optimized" PV devices, i.e., i) they are devices with "poor" contact geometries; and ii) they are illuminated through absorbing μc-Si p-layers that were deposited onto the ITO-coated glass substrates.

We have also fabricated p-i-n structures with μc-Si,C p-layers grown from 0.1% diborane source gas mixtures, using an $SiH_4/(SiH_4 + CH_4)$ ratio = 0.67. These structures employed heavily doped μc-Si n-layers, and had a-Si:H i-layers. The n and p-layer thicknesses were 150 and 300Å, respectively, and the i-layer thicknesses were 3000Å and 4000Å. The structures were deposited onto ITO-coated glass substrates and illuminated through the p-regions. Open circuit voltages were 0.6 eV, and the short circuit current density, under approximately 0.5 AM1 illumination - 50 mW/cm^2 from quartz halogen lamp, were respectively 5.2 and 8.1 mA/cm^2 for the devices with the 3000Å and 4000Å thick i-layers.

C.3. MOS Device Structures using Doped a-Si:H and μc-Si

We have studied the properties of doped a-Si:H and μc-Si in MOS capacitors using ~10 W-cm p-type crystalline substrates and thermally grown SiO_2 dielectric layers. These studies have provided information about the relative electron affinities of a-Si:H and μc-Si, and the effective Debye lengths in μc-Si films with different levels of p-type and n-type doping. This information is important in the design of solar cell structures that utilize the doped a-Si:H or doped μc-Si in the p- and n-layers of p-i-n structures.

We have expanded these studies of μc-Si as a gate electrode material, and have compared the properties of n^+ and p^+ μc-Si, with respective conductivities of ~50-100 S/cm and 6-10 S/cm, onto thermally-grown and remote PECVD SiO_2 films. The remote PECVD SiO_2 films were subjected to a post-deposition anneal prior to μc-Si depositions. C-V measurements established that changing from n^+ to p^+ μc-Si electrodes produced a 0.8 eV shift of the flatband voltage for both types of oxides. This provides a measure of the Fermi level difference between the n^+ and p^+ μc-Si, and has implications for the maximum values of the open circuit voltages using μc-Si

materials as the n^+ to p^+ layers in p-i-n photovoltaic devices.

D. Theory and modelling

D.1. Effects of Disorder on Electronic States in a-Si:H

D.1.1. Bond and dihedral angle distortions

There is a large body of experimental evidence that has identified the dominant bonding defects in a-Si:H films as dangling bonds. Experiments, and in some cases theory, have further demonstrated that i) the exact positions of neutral dangling bonds in the band-gap of a-Si:H are modified in a systematic way by the incorporation of strongly electronegative alloy (or impurity) atoms, C, N, and O; the higher the electronegativity, the closer to the conduction band edge (this model prediction has been verified by the experiments of Dave Cohen and coworkers), ii) that the defects generated via light-soaking, and stress-bias are also dangling bonds, and iii) that the parentage of the defects generated by light-soaking, and/or stress-biasing may indeed be *weak and/or strained bonds* within the a-Si:H network structure. The issue that has not been resolved relates to the exact nature of these weak and/or strained bonds, and the extent to which the processes that promote their conversion to defects, and/or their relaxation during annealing involve H-atom migration and/or bonding.

The tight-binding approach have been extended to include two different tight-binding models, and to investigate the effects of both bond-angle, and dihedral angle disorder on the band edge density of electronic states. These studies have shown that using a Hamiltonian with i) only nearest neighbor interactions, and ii) the *empirically-constructed* sp^3s^* basis set of Dow and co-workers, yields qualitatively different results than using a Hamiltonian with i) nearest and second-nearest neighbor interactions; and ii) a set of tight-binding parameters that generates a good band-structure for crystalline Si with an sp^3 basis set. This comparison identifies a fundamental limitation in using semi-empirical tight-binding methods.

A study of modifications in the electronic states associated with bond-angle deviations from the ideal tetrahedral geometry has been completed, and using a nearest neighbor Hamiltonian has been been completed. The objective was to determine whether bonding configurations with large bond-angle deviations could be the origin of the weak bonds that eventually contribute to defect generation via light-

soaking or stress bias. Figure 4 shows the effect of bond-angle distortions on the valence and conduction band edges. These calculations were restricted to two-body interactions, and used an sp^3s^* basis set. The results of these calculations, computed from Bethe Lattices with statistical distributions of angular distortions, demonstrate that as the average bond-angle deviations increase, the gap narrows with the major contribution to the narrowing being broadening at the valence band edge. The calculations for isolated clusters, connected to ideal Si Bethe Lattices indicate that bond-angle deviations greater than about 20 degrees can lead to the generation of localized states. We have studied electronic states associated with bond-angle deviations from an ideal tetrahedral geometry. Our objective is to determine whether bonding configurations with large bond-angle deviations are the origin of the weak bonds that eventually contribute to defect generation via light-soaking or stress bias. Our initial calculations used nearest neighbor interactions, an sp^3s^* basis set, and averaged over Bethe lattices in which all bonds were distorted. These calculations indicated that as the average bond-angle deviation is increased, the gap narrows with the major contribution to the narrowing being a broadening, and tailing into the gap at the valence band edge. There is very little movement or change in the conduction band edge in this model calculation. We have also performed calculations for isolated clusters with bond-angle distortions; these are terminated with ideal Si Bethe Lattices. These calculations indicate that bond-angle deviations greater than about 20 degrees can lead to the generation of localized states that emerge from the valence band edge.

We have also studied the effects of bond-angle distortions using a Hamiltonian that includes second neighbor interactions, and have used an sp^3 basis set for these calculations. The parameters for this calculation are obtained from the application of the same Hamiltonian to crystalline silicon, where it yields excellent results for both the valence and conduction bands. The application of this Hamiltonian to a Bethe Lattice structure with no bond angle distortions, and a single "idealized" dihedral angle, gives an excellent representation of both the valence and conduction band structures for a-Si. This is the same result we found for the sp^3s^* basis set and nearest neighbor interactions, indicating the "non-uniqueness" of these model calculations.

We have also used the second-neighbor Hamiltonian to calculate the band structure for Bethe Lattices that included statistical distributions of bond-angle distortions. There are two important results that we have found i) the effective band-gap decreases as the average bond angle distortion increases; and ii) the band-gap

penetration at the conduction and valence band edges are about the same. The first of these results is similar to what has been found in the tight-binding calculations that used only nearest neighbor interactions, and the sp^3s^* basis set. However, the second observation is qualitatively and and quantitatively different. In particular we find that as the valence band edge moves into the forbidden gap, the edge softens, whereas as the conduction band edge moves into the gap, the edge sharpens.

Therefore the results of both models support the idea that the slope of the absorption edge in the exponential region is determined primarily by the valence band edge. Both models also support the interpretations of transport data which indicate the dispersion at the conduction band edge is less than at the valence band edge. In this instance, the nearest neighbor interaction model, using the sp^3s^* basis set, over-estimates the ratio of band tailing effects; i.e., the calculated ratios are about three to one, whilst the experimentally estimated ratios are less than two to one. Overall, it appears that a Hamiltonian with second neighbor interactions and an sp^3 basis set provides a better starting point for model calculations of weak bonds, and other types of defects, e.g., dangling bonds as well.

We have also applied a tight-binding model to Si-Bethe lattice structures in order to investigate the effects of bond-angle, and/or dihedral angle disorder. We have used a Hamiltonian with nearest and second-nearest neighbor interactions, and have been able to identify and separate the effects bond angle disorder and dihedral angle disorder on the states at the states at the conduction and valence band edges. We have systematically investigated the formation of electronic states in the region of the conduction and valence band edges of a-Si as functions of variations in the bond and dihedral angle distributions. Local Density of States (LDOS) for Si atoms in disordered environments have been calculated using the cluster Bethe lattice method with a tight-binding Hamiltonian containing both first and second nearest neighbor interaction terms. We conclude that the change in orbital overlap, incurred from rotations about the axes defining the dihedral angle distortions, is the origin of the effect of dihedral angle disorder on the electronic states near the band gap.

Short range disorder in a-Si can effect the electronic density of states (DOS) near the band edges, shift the band edges or create discrete states in the band gap. We have made a study of short range disorder arising from bond angle distortions on the DOS of a-Si near the band edges. Raman scattering studies of a-Si and a-Ge by

Lannin have related the bond angle disorder to a shift in the optical energy gap. Previous studies using a tight-binding approach have shown valence band states for individual atoms in distorted tetrahedral environments, or have estimated the bounds for band tailing due to bond and dihedral angle distortions. The Hamiltonians in these studies were restricted to nearest neighbor interactions, whereas our calculations have been performed with a tight-binding Hamiltonian that includes both first and second neighbor interaction terms.

Bond angle distortions and dihedral angle variations in clusters embedded in a Bethe lattice show effects on the LDOS at the top of the valence and at the bottom of the conduction band. Both E and F mode distortions increase the states at the edge of the conduction and valence band for the staggered configurations. Rotation of the dihedral angles to the eclipsed configurations can reduce the magnitude of states at the band edges by pushing these states farther into the band. This effect cannot be seen with a nearest neighbor Hamiltonian, which can model the bond angle distortions adequately, but cannot account for changes in distance and symmetry of the outer shells of atoms due to intermediate range disorder such as the dihedral angle variations. A key component of modeling the dihedral angle distortion are the 2nd neighbor interaction terms and the distance scaling law used with them. We are currently investigating other tight-binding parameters to determine the sensitivity of these results to the empirical fit of the terms and their relationship to neighbor distance on the band structure of Si.

D.1.2. Bond-Angle Disorder Effects in a-Si:H and a-Si,Ge:H

These model calculations have demonstrated that bond-angle distortions, present in a-Si:H, and a-Si,Ge:H, play a significant role in determining the energies of localized states with in the gap. We have found two situations where the effects of bond-angle distortions are different, but equally important with respect to their effects on either generating localized states, or producing a spread in their energies. For the a-Si:H system, we have shown that bond-angle distortions can shift the energy of the Si-H anti-bonding state out of the conduction band, and thereby generate a localized state that has all of the attributes of the floating bond state first described by Pantelides. This state can trap an electron, and then play a role in defect related photo-transport properties such as the Stabler-Wronski effect. Since relative large bond-angle distortions, ~16° or more, are required to move these states into the

bandgap, their numbers will be small with respect to the density of bonded H-atoms, but is none-the-less sufficiently large, at least of the order of 10^{16} to 10^{18} cm^{-3}, to have an effect on the electronic properties.

We have also shown that bond-angle disorder produces an energy spread in the Si-atom and Ge-atom dangling bonds in a-Si,Ge:H alloys, and that this spread in energies is sufficient to cause the respective dangling bond distributions to overlap in energy. The separation between these dangling bond states in idealized tetrahedral networks, and using a valence band offset energy of ~0.20 eV, is ~0.13 ± 0.02 eV, depending on the alloy composition, and including the effects of different distributions of nearest-neighbor Si and Ge-atoms. On the other hand energy level broadening of ~0.3 eV or more will occur for bond-angle deviations of the order of 6°-8° which is characteristic of fully relaxed amorphous networks. This conclusion remains unchanged even if the Ge-atom dangling bond energy is higher in the gap by ~0.1 eV, as predicted from the band offset of ~0.55 eV for strained Si/Ge heterojunctions.

D.2. Dangling Bonds in a-Si,Ge:H alloys

We have used an empirical tight-binding approach to determine the relative energies of Si and Ge dangling bonds in a-Si. These calculations use a Bethe lattice structural model, and an sp^3s^* Hamiltonian, with only nearest We maintain perfect tetrahedral geometry at the dangling bond sites, and within the Bethe lattice as well. The self-energies of the Si and Ge atoms have been adjusted to give the experimentally determined valence band offset energy of ~0.2 eV. We find that a Ge-atom dangling bond, with three back-bonded Si-atoms, is about 0.1 eV lower in energy that a Si-atom dangling bond, also back-bonded to three Si-atoms. These calculations are being extended i) to Si and Ge atoms with different number of Si and Ge atoms as their immediate neighbors, and with Bethe lattice terminations to these local clusters that are appropriate to a-Si,Ge alloys; and ii) to include bond and dihedral angle distortions at the dangling bond sites.

D.3. Bond-energies and Vibrational-frequencies of Si-H groups

We have used ab initio and empirical calculations to study non-random bonding arrangements in a-Si,O:H and doped a-Si:H films. The two approaches give comparable results for the bond energies of SiH groups that are near-neighbors to the

oxygen and dopant atoms. The calculations have been used to develop a model for the way in which these bonding arrangements are created in thin film deposition processes in which surface, rather than gas phase reactions dominate for the range of deposition parameters used to produce electronic or device grade materials.

We have identified several important *non-statistical* bonding environments in alloyed and doped a-Si:H. These include O-Si-H *linkages* in a-Si,O:H alloys, and P^+-Si-H and Si-B^--H *linkages* that play a significant role in the doping processes in a-Si:H. We present the experimental evidence for these bonding arrangements, and a model that accounts for their creation during film deposition.

Bond energies have been determined in two ways for 3 bonding configurations that include Si, O and H: 3Si-SiH, 2Si,O-SiH and 3O-SiH. This was done i) using empirical relationships based on differences in electronegativities; and ii) by ab-initio calculations applied to hydrogen-terminated clusters that contain the SiH group, but with different numbers of Si- and O-atoms back-bonded to the Si-atom of that group.

The calculated Si-H energies are given below:

Group	Bond Energy (eV) (Relative Energy)			
	Ab-initio Calculation		Empirical Calculation	
3Si-SiH	4.06	(1.00)	3.92	(1.00)
2Si,O-SiH	4.21	(1.04)	4.14	(1.06)
3O-SiH	4.66	(1.15)	4.64	(1.18)

The bond-energies, normalized to 3Si-SiH, demonstrate that both approaches yield similar relative bond-energies for the three groups.

Ab-initio calculations have not as yet been performed on clusters that include the charged and electrically active P^+ and B^- dopant atoms. We have estimated bond energies for these configurations using the empirical approach based on electronegativities. We first compute bond energies for some of the probable bonding arrangements involving H-atoms, and then for the case of the P-atom bonding environments establish a *chemical equivalence* between the O-Si-H and P^+-Si-H *linkages* through a calculation of the *partial charge* on the Si and H atoms. The empirically determined bond energies are given below:

Group	Bond Energy (eV)	Relative Energy
2Si,P^+-SiH	4.37	1.00
2Si-PH	4.18	0.96

3Si,B^--H	4.56	1.00
2Si-BH	4.99	1.09

The calculation of partial charges below establishes a *linkage* between these empirical bond energy calculations, and the ab-initio and empirical calculations presented above:

Bonding Group	Si Charge	H Charge
3Si-SiH	+ 0.04 e	- 0.15 e
2Si,O-SiH	+ 0.15 e	- 0.05 e
2Si,P^+-SiH	+ 0.19 e	- 0.02 e

Partial charges obtained from ab-initio calculations give equivalent trends for the first two groups. The partial charges on the Si- and H-atoms for the 2Si,O-SiH and 2Si,P^+-SiH groups are similar, and therefore exhibit *equivalent* differences with respect to the corresponding partial charges of the 3Si-SiH group. In the spirit of the empirical models, this implies comparable bond energies for these SiH groups, and therefore similar differences with respect to bond energy of the SiH group in the 3Si-SiH cluster. This is supported by the bond energies calculations that we have presented above.

a-Si,O:H alloys are typically deposited at temperatures between 225 and 300°C. Film growth proceeds from a heavily hydrogenated surface, so that differences in the bonded H-concentrations derive from the rate at which H atoms are thermally *removed* from that growth surface. Since bond energies of all relevant SiH groups are of the order of 4 eV, the relatively small differences between these bond-energies, ~0.2 eV, for SiH in 3Si-SiH, and in 2Si,O-SiH clusters cannot completely account for the preferential retention of H in 2Si,O-SiH arrangements.

It has been shown that H-atoms initially bonded to a crystalline Si surface, can be removed from that surface at low temperatures by exposure to atomic hydrogen. This is followed by some type of surface reconstruction, as in the transition from a dihydride H-terminated Si(100) surface with 1x1 symmetry to an SiH-terminated surface with a 2x1 symmetry: surface dihydride groups are converted to monohydride groups, and a Si-Si dimer bond is formed.

We propose that plasma generated H-atoms (or protons) play a similar role in H-removal from hydrogen-terminated a-Si surfaces during film deposition. The rate limiting step for a surface reaction is often through the creation of an intermediate arrangement in which the Si surface atom is over-coordinated as in 3Si-Si-2H. This

surface structure is energetically unstable with respect to interaction with an SiH_3 group. The rate of attachment of H, that creates the over-coordination will depend on the partial charge on the Si atom, and whether the H that is to be attached is an atom or a proton. If we assume that protons are the active species, then the rate of attachment is expected to decrease as the partial charge on the Si atom of the surface bonding group increases and becomes more positive. This factor could account for the increased stability of the bonding arrangements involving O and P^+ atoms.

Based on the experimental studies of a-Si,O:H, and P and B-doped a-Si:H, there are local bonding environments involving Si and H atoms with either O, P or B atoms that are non-statistical in the sense that they would not be anticipated solely by the relative concentrations of these atoms in the films. This infers that there are chemical driving forces for their creation in the deposited films. Since SiH groups, as well as OH, PH and BH groups all have bonding energies of about 4 eV, small differences in these energies by themselves cannot account for preferential formation of SiH or B^-H bonding groups for films deposited at 200-300°C. This leads us to propose a mechanism for the occurrence of the non-statistical bonding arrangements that is related to surface reaction chemistry. The model includes three steps i) the formation of an intermediate structure in which the Si, and/or B or P atoms are over-coordinated by additional H-atoms; ii) the break-up of these surface intermediates through the release of molecular H - H_2; and iii) the attachment of an SiH_n group that continues the film growth process. In addition to these bonding sites involving H atoms and the dopant atoms P and B, there are other bonding groups in which P and B are threefold-coordinated and inactive with respect to doping. In this context, the calculated relative bonding energies for the *doping and inactive groups* are in accord the observation that the doping efficiency for P-atoms is significantly higher than for B-atoms.

Figure Captions.

Figure 1. Absorption constant versus substrate temperature (a) GD a-Si:H, and (b) RPECVD a-Si:H).

Figure 2. Mono- and poly-hydride versus total bonded-H (a) GD a-Si:H, and (b) RPECVD a-Si:H).

Figure 3. Dark and photoconductivity for B-doped μc-Si versus (a) dark conductivity activation energy, and (b) boron concentration as determined by SIMS.

Figure 4. Meyer-Neldel plot of conductivity prefactor versus activation energy.

Figure 5. Room temperature conductivity versus dark conductivity activation energy.

Figure 6. Activation energy for Si,C versus activation energy for Si.

Figure 7. Band-alignment diagrams between Si-crystallites and (a) a-Si:H, and (b) a-Si,C:H. and for light and heavy doping for (c) μc-Si and (d) μc-Si,C.

Figure 8. Barrier transport mechanisms for μc-Si, and μc-Si,C.

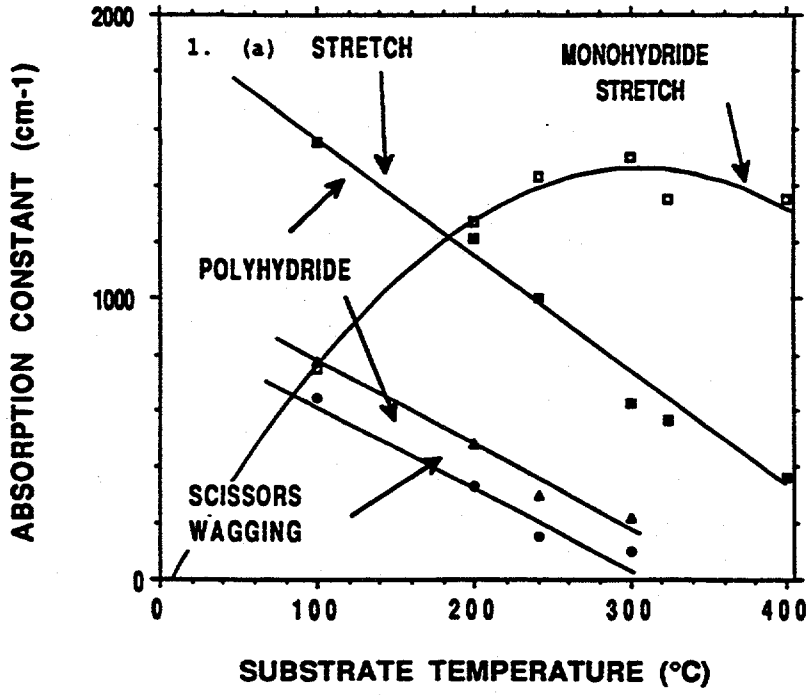
1. (a) STRETCH
MONOHYDRIDE STRETCH
POLYHYDRIDE
SCISSORS WAGGING
ABSORPTION CONSTANT (cm-1)
2000
1000
0
0
100
200
300
400
SUBSTRATE TEMPERATURE (°C)

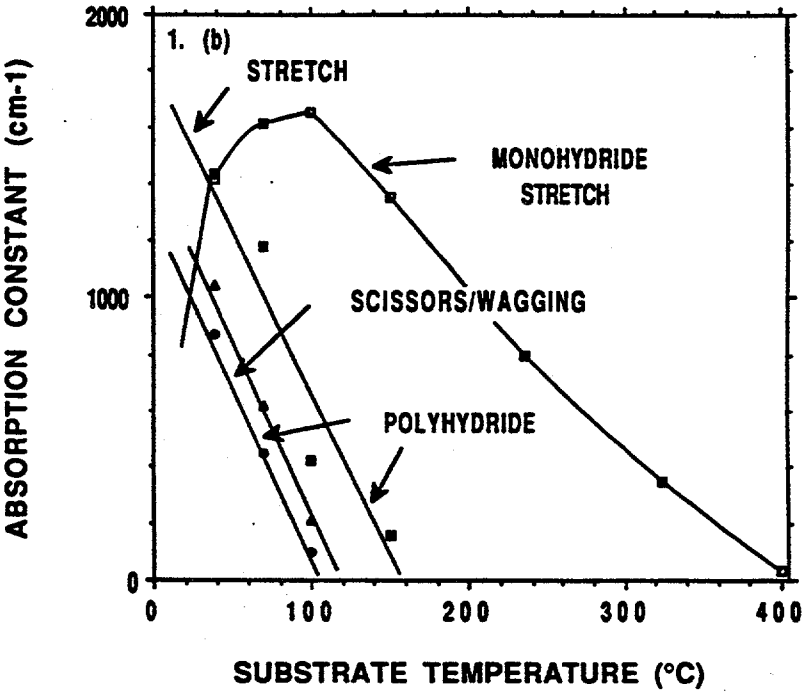
1. (b)
STRETCH
MONOHYDRIDE STRETCH
SCISSORS/WAGGING
POLYHYDRIDE
ABSORPTION CONSTANT (cm-1)
2000
1000
0
0
100
200
300
400
SUBSTRATE TEMPERATURE (°C)

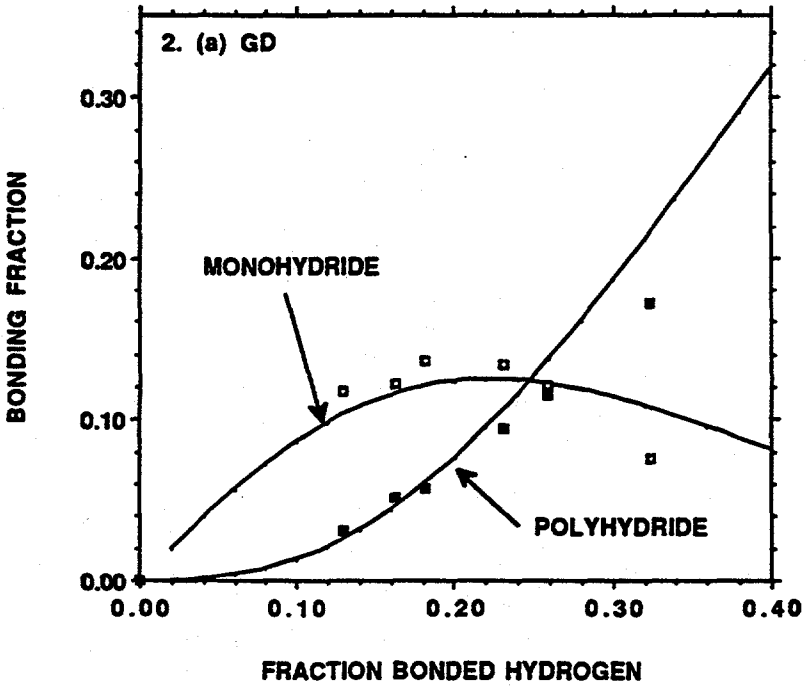
2. (a) GD
0.30
0.20
0.10
0.00
MONOHYDRIDE
POLYHYDRIDE
BONDING FRACTION
0.00
0.10
0.20
0.30
0.40
FRACTION BONDED HYDROGEN

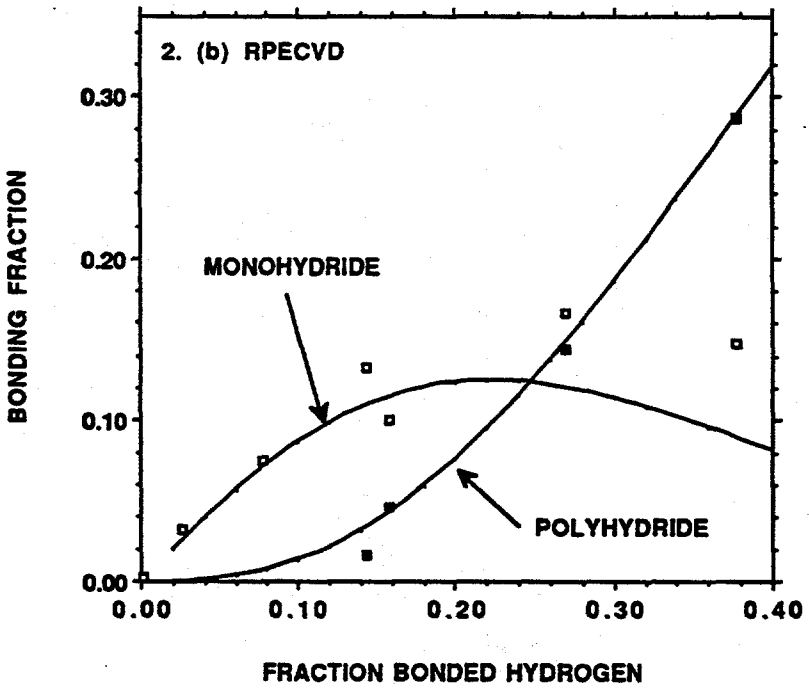
2. (b) RPECVD
0.30
0.20
0.10
0.00
MONOHYDRIDE
POLYHYDRIDE
BONDING FRACTION
0.00
0.10
0.20
0.30
0.40
FRACTION BONDED HYDROGEN

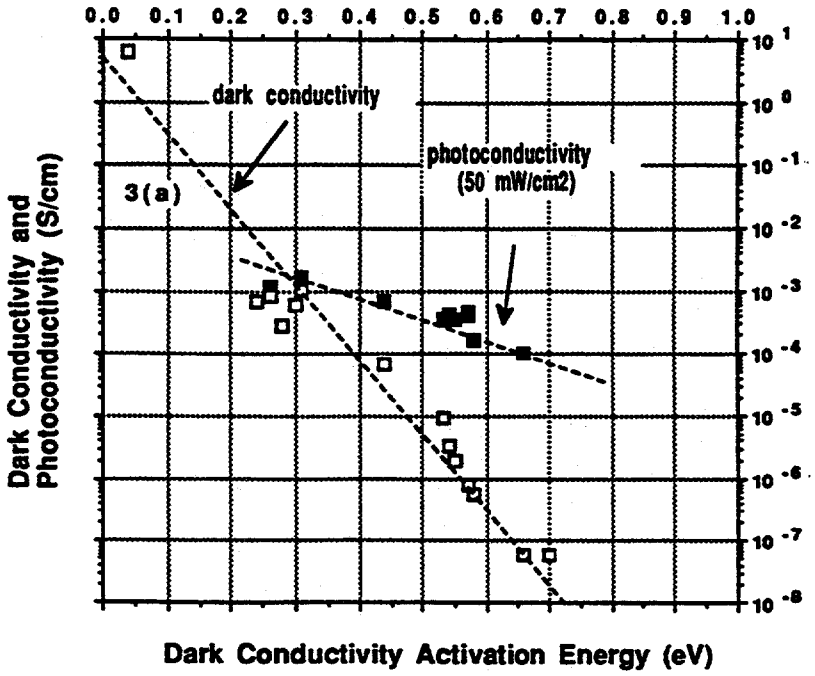
0.0 0.1 0.2 0.3 0.4 0.5 0.6 0.7 0.8 0.9 1.0
10 1
10 0
10 -1
10 -2
10 -3
10 -4
10 -5
10 -6
10 -7
10 -8
dark conductivity
photoconductivity
(50 mW/cm2)
3(a)
Dark Conductivity and
Photoconductivity (S/cm)
Dark Conductivity Activation Energy (eV)

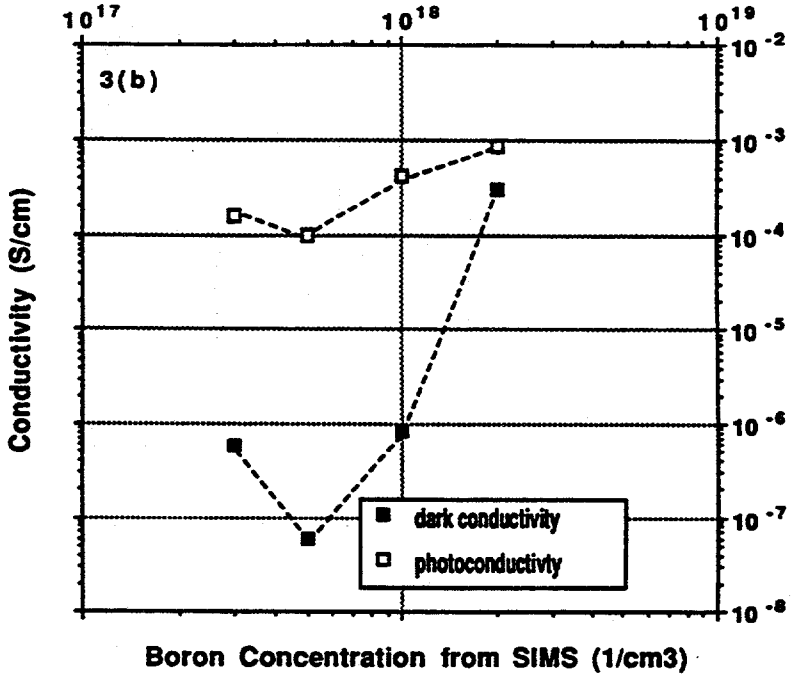
10 17
10 18
10 19
10 -2
10 -3
10 -4
10 -5
10 -6
10 -7
10 -8
3(b)
dark conductivity
photoconductivity
Conductivity (S/cm)
Boron Concentration from SIMS (1/cm3)

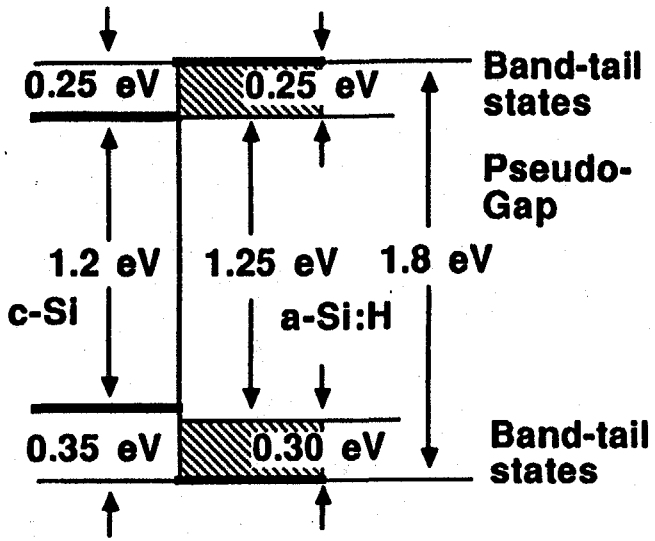
0.25 eV
0.25 eV
Band-tail states
Pseudo-Gap
1.2 eV
1.25 eV
1.8 eV
c-Si
a-Si:H
0.35 eV
0.30 eV
Band-tail states

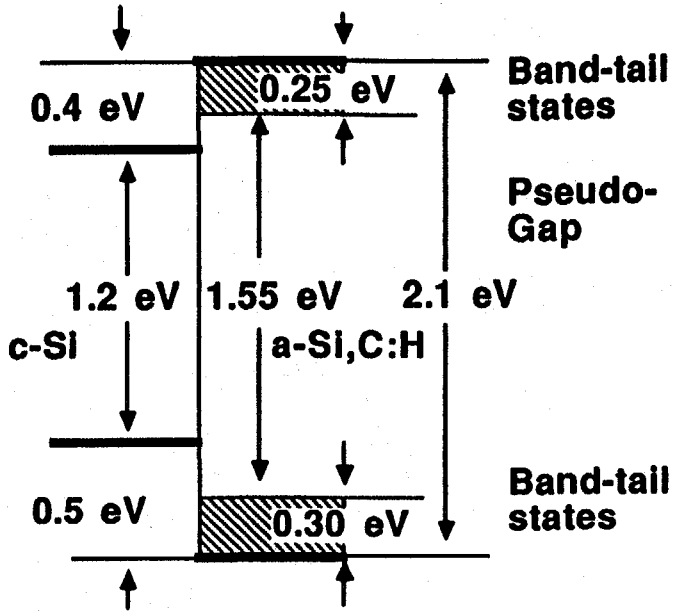
0.4 eV
0.25 eV
Band-tail states
Pseudo-Gap
1.2 eV
1.55 eV
2.1 eV
c-Si
a-Si,C:H
0.5 eV
0.30 eV
Band-tail states

7 (a) and (b)

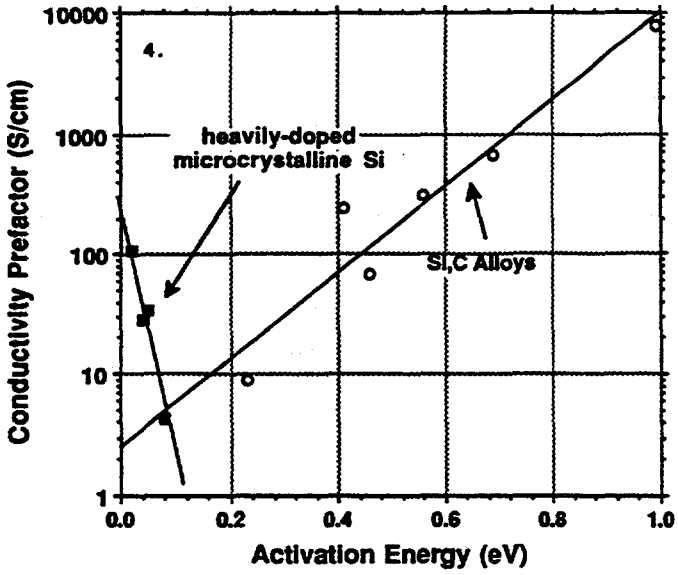
4.
heavily-doped
microcrystalline Si
Si,C Alloys
Conductivity Prefactor (S/cm)
Activation Energy (eV)
10000
1000
100
10
1
0.0
0.2
0.4
0.6
0.8
1.0

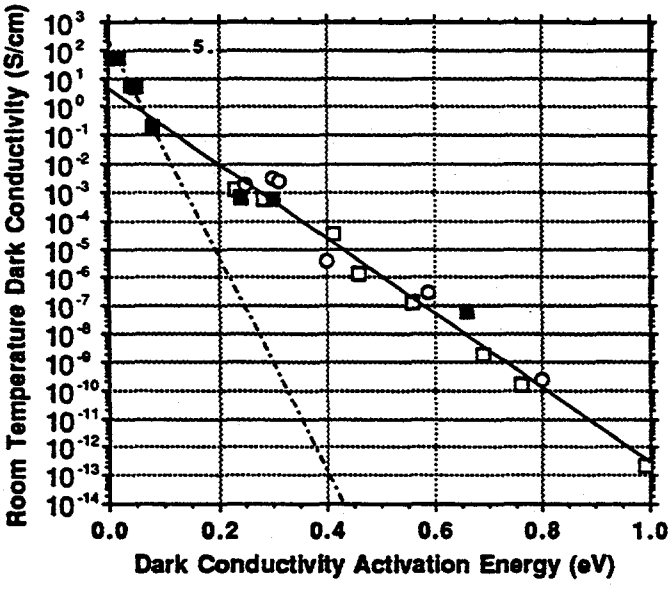
5.
Room Temperature Dark Conductivity (S/cm)
Dark Conductivity Activation Energy (eV)
0.0
0.2
0.4
0.6
0.8
1.0

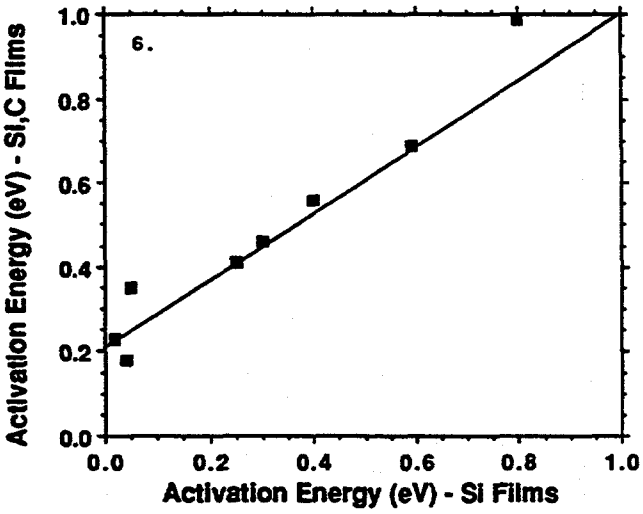
6.
Activation Energy (eV) - Si,C Films
Activation Energy (eV) - Si Films
0.0
0.2
0.4
0.6
0.8
1.0

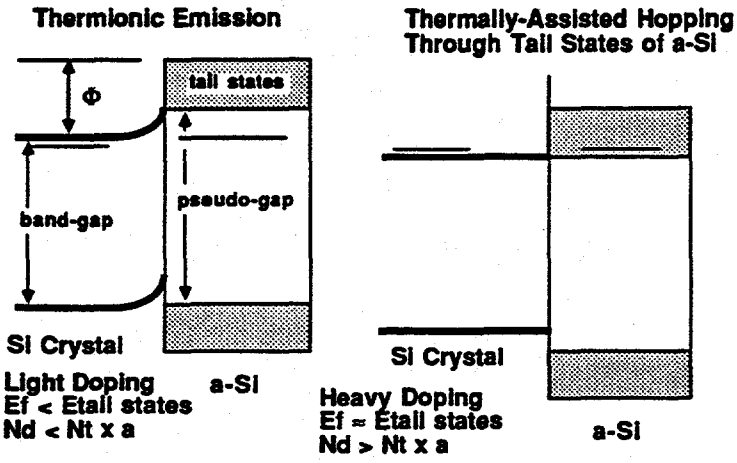
Thermionic Emission
Thermally-Assisted Hopping
Through Tail States of a-Si
Φ
tail states
band-gap
pseudo-gap
Si Crystal
Light Doping
Ef < Etail states
Nd < Nt x a
a-Si
Si Crystal
Heavy Doping
Ef ≈ Etail states
Nd > Nt x a
a-Si

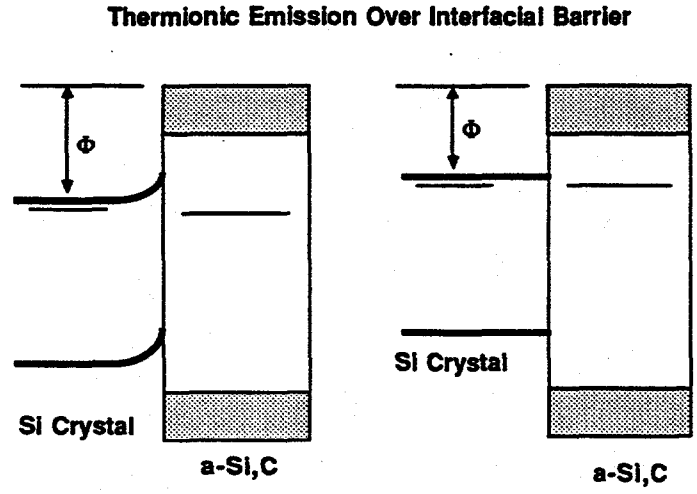
Thermionic Emission Over Interfacial Barrier
Φ
Si Crystal
a-Si,C
Φ
Si Crystal
a-Si,C
For Both Light and Heavy Doping
Ef < Etail states so that Band Off-Set
at a-Si,C Interface Dominates

7(c) and (d)

Thermionic Emission

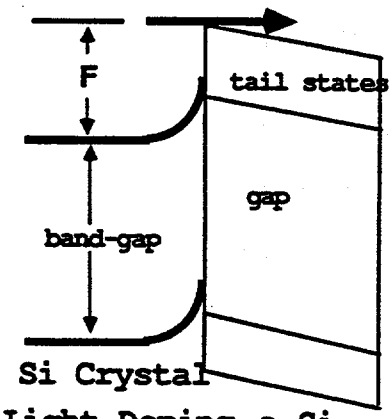

Light Doping a-Si

Thermally-Assisted Tunnelling
Through Band-Tail States of a-Si

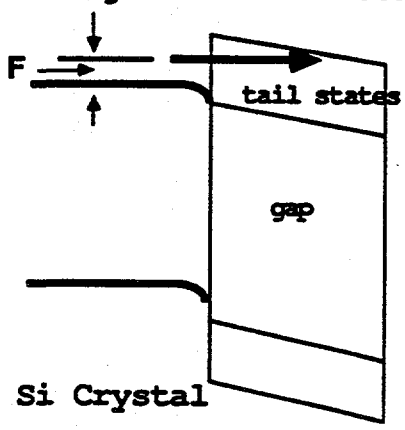

Heavy Doping a-Si

Thermionic Emission Over Interfacial Barrier

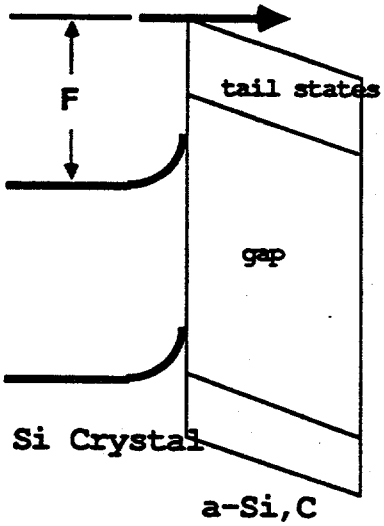

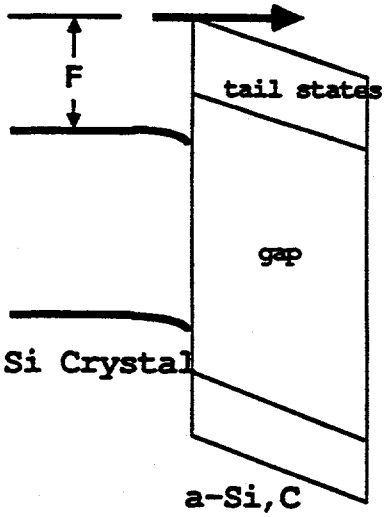

Light and Heavy Doping

III. RESEARCH PUBLICATIONS

This section of the report lists the publications between 1989 and 1992, that have resulted from this research sub-contract. This section has been organized according the publication year, i.e., 1989, 1990, etc.

1989

G. Lucovsky, G.N. Parsons, C. Wang, B.N. Davidson and D.V. Tsu, "Low Temperature Deposition of Hydrogenated Amorphous Silicon: Control of Polyhydride Incorporation and its Effects on Thin Film Properties", Solar Cells **27**, 121 (1989).

B.N. Davidson, G. Lucovsky, G.N. Parsons, R.J. Nemanich, A. Esser, K. Seibert, and H. Kurz, "Free Carrier Absorption and the Transient Optical Properties of Amorphous Silicon Thin Films: A Model Including Time-Dependent Free-Carrier, and Static, Dispersive Interband Contributions to the Complex Dielectric Constant", J. Non-Cryst. Solids **114**, 579 (1989).

A. Esser, K. Seibert, H. Kurz, G.N. Parsons, C. Wang, B.N. Davidson, G. Lucovsky and R.J. Nemanich, "Ultrafast Recombination and Trapping in Amorphous Silicon", J. Non-Cryst. Solids **114**, 573 (1989).

G.N. Parsons, C. Wang, M.J. Williams, and G. Lucovsky, "Reduction of Defects by High Temperature Annealing (150°C-240°C) in Hydrogenated Amorphous Silicon Films Deposited at Room Temperature", J. Non-Cryst. Solids **114**, 178 (1989).

G. Lucovsky, B.N. Davidson, G.N. Parsons and C. Wang, "Incorporation of Polyhydride Bonding Groups into Thin Films of Hydrogenated Amorphous Silicon (a-Si:H)", J. Non-Cryst. Solids **114**, 154 (1989).

D.V. Tsu and G. Lucovsky, "SiH Stretching Vibrations in Silicon Suboxides: Local and Remote Induction Effects", J. Non-Cryst. Solids **114**, 501 (1989).

C. Wang, G.N. Parsons and G. Lucovsky, "Effects of gas additives on the properties of sputtered a-Si:H films", J. Non-Cryst. Solids **114**, 193 (1989).

Z. Yin, D.V. Tsu, G. Lucovsky and F.W. Smith, "Annealing Study of the Infrared Absorption in an Amorphous Silicon Dioxide Film", J. Non-Cryst. Solids **114**, 4579 (1989).

R.J. Nemanich, E.C. Buehler, Y.M. LeGrice, R.E. Shroder, G.N. Parsons, C. Wang, G. Lucovsky and J.B. Boyce, "Raman Scattering from Microcrystalline Si Films: Considerations of Composite Structures with Different Absorption Constants", J. Non-Cryst. Solids **114**, 813 (1989).

S.S. Kim, G.N. Parsons, G.G. Fountain, and G. Lucovsky, "Dependence of a-Si:H/Si_3N_4 Interface properties on the Deposition Sequence in the Amorphous silicon thin film transistors produced by remote PECVD process", J. Non-Cryst. Solids **115**, 69 (1989).

G. Lucovsky and G.N. Parsons, "Deposition and Thermal Annealing of Device-Quality Hydrogenated Amorphous Silicon (a-Si:H) Thin Films at Low Processing Temperatures (T_s, T_{an} < 200°C)", Optoelectronics **24**, 119 (1989).

G.N. Parsons, D.V. Tsu and G. Lucovsky, "Defects in a-Si:H films produced by remote plasma enhanced CVD (RPECVD)" J. Non-Cryst. Solids **107**, 295 (1989).

G.N. Parsons, D.V. Tsu C. Wang and G. Lucovsky, "Precursors for the deposition of amorphous silicon hydrogen alloys by remote plasma enhanced CVD", J. Vac. Sci. Technol. **A7**, 1124 (1989).

G.N. Parsons, D.V. Tsu and G. Lucovsky, "Chemical reaction pathways for the deposition of a-Si:H films by remote plasma enhanced chemical vapor deposition", MRS. Symp. Proc. **131**, 263 (1989).

C. Wang, G.N. Parsons and G. Lucovsky, "Suppression of Polyhydride Bonding in Magnetron Sputtered a-Si:H Alloys Using Water Vapor", MRS Symp. Proc. **149**, 75 (1989).

G.N. Parsons, S.S. Kim and G. Lucovsky, "Substrate Interactions in The Formation of Amorphous Silicon/Dielectric Interfaces for FET Device Structures", MRS Symp. Proc. **149**, 263 (1989).

1990

G.N. Parsons and G. Lucovsky, "Silicon-Hydrogen Bond-Stretching Vibrations in Hydrogenated Silicon, Nitrogen Alloys", Phys. Rev. **B41**,,1664 (1990).

G.N. Parsons, C. Wang, M.J. Williams and G. Lucovsky, " Post-deposition Relaxation of Electronic Defects in Hydrogenated Amorphous Silicon", Appl. Phys. Lett. **56**, 1895 (1990).

A. Esser, K. Seibert and H. Kurz, G.N. Parsons, C. Wang, B.N. Davidson, G. Lucovsky, and R.J. Nemanich, "Ultrafast Recombination and Trapping in Amorphous Silicon", Phys. Rev. **B41** (1990).

G.N. Parsons and G. Lucovsky, "Nitrogen Incorporation Reactions in Hydrogenated Amorphous Silicon, Nitrogen Alloys Produced by Remote PECVD", MRS Symp. Proc. **165**, 85 (1990).

B.N. Davidson, G.N. Parsons, C. Wang and G. Lucovsky, "Polyhydride Bonding Groups in PECVD Amorphous Silicon Thin Films", MRS Symp. Proc. **165**, 173 (1990).

C. Wang, G.N. Parsons, E.C. Buehler, G. Lucovsky and R.J. Nemanich, "Substrate Temperature Dependence of the Raman Spectra for Microcrystalline Silicon Films Produced by Reactive Magnetron Sputtering", MRS Symp. Proc. **164**, 21 (1990).

R.J. Nemanich, E.C. Buehler, Y.M LeGrice, R.E. Schroder, G.N. Parsons, C. Wang, G. Lucovsky and J.B. Boyce, "Raman Scattering from Microcrystalline Films: Considerations of Composite Structures with Different Optical Absorption Properties, MRS Symp. Proc. **164**, 265 (1990).

C. Wang, G.N. Parsons and G. Lucovsky. "Microcrystalline Silicon thin Film Deposited by Reactive Magnetron Sputtering and Remote Plasma enhanced Chemical Vapor Deposition Process", MRS Symp. Proc. **192**, 535 (1990).

G.N. Parsons, C. Wang and G. Lucovsky. "Reduction of Electronic Defects by

Annealing in Hydrogenated and Unhydrogenated Amorphous Silicon", MRS Symp. Proc. **192**, 775 (1990).

S.S. Kim, C. Wang, G.N. Parsons and G. Lucovsky. "a-Si:H Thin Film Transistors and Logic Circuits Fabricated in an Integrated Multichamber System", MRS Symp. Proc. **192**, 373 (1990).

B. N. Davidson and G. Lucovsky, "Electronic states in the gap of a-Si from bond angle variations.", MRS Symp. Proc. **192**, 279 (1990).

G.N. Parsons, C. Wang and G. Lucovsky, "Annealing of "Intrinsic" and Photo-induced Defects in Hydrogenated Amorphous Si, a-Si:H, Thin Films", Thin Solid Films **193&194**, 577 (1990).

1991

C. Wang, M.J. Williams and G. Lucovsky, "Preparation of Microcrystalline Silicon Thin Films by Remote PECVD", J. Vac. Sci. Technol. **A9**, 444 (1991).

G. Lucovsky, C. Wang, R.J. Nemanich and M.J. Williams, "Deposition of μc-Si and μc-Si,C Thin Films by Remote Plasma-Enhanced Chemical-Vapor Deposition", Solar Cells **30**, 419 (1991).

D.R. Lee, C.H. Bjorkman, and G. Lucovsky, "Effective Electron Affinities in Doped a-Si:H and μc-Si Films as Determined from Studies of MOS Capacitors," J. of Non-Cryst. Solids **137&138**, 1059 (1991).

B.N. Davidson, G. Lucovsky, and J. Bernholc, "Effect of the Local Disorder in a-Si on the Electronic Density of States Near the Band Edges", J. of Non-Cryst. Solids **137&138**, 307 (1991).

G. Lucovsky, Z. Jing and J.L. Whitten, "Chemical Induction Effects: O-incorporation in, and Substitutional Doping of a-Si:H", J. of Non-Cryst. Solids **137&138**, 119 (1991).

A. Esser, H. Heesel, H.Kurz, C. Wang, M.J. Williams and G. Lucovsky, "The Role of Dangling Bond States in the Picosecond Recovery of Photoinduced Absorption in a-Si:H", J. of Non-Cryst. Solids **137&138**, 535 (1991).

C. Wang, G. Lucovsky and R.J. Nemanich, "Preparation and Properties of Doped a-

Si,C:H and μc-Si,C Alloy Films by Remote PECVD", J. of Non-Cryst. Solids **137&138**,741 (1991).

M.J. Williams, Cheng Wang, and G. Lucovsky, "Photoconductivity and Optical Stability of Intrinsic mc-Si Films Formed by Remote Plasma Enhanced Chemical Vapor Deposition, Remote PECVD", J. of Non-Cryst. Solids **137&138**, 737 (1991).

D.R. Lee, C.H. Bjorkman, C. Wang, and G. Lucovsky, "Studies of MOS and Heterojunction Devices Using Doped μc-Si and a-Si," MRS Symp. Proc. **219**, 395 (1991).

C. Wang, G. Lucovsky and R.J. Nemanich, "Deposition of the Amorphous and Microcrystalline Si,C Alloy Films by Remote PECVD Process", MRS Symp. Proc. **219**, 751 (1991).

M.J. Williams, C. Wang, and G. Lucovsky, "Deposition and Characterization of Near "Intrinsic" mc-Si Films Deposited by Remote Plasma Enhanced Chemical Vapor Deposition", MRS Symp. Proc. **219**, 389 (1991).

G. Lucovsky and C. Wang, "Barrier Limited Transport Mechanisms in Doped mc-Si and μc-Si,C", MRS Symp. Proc. **219**, 377 (1991).

B.N. Davidson, G. Lucovsky, and J. Bernholc, "Effect of the Local Disorder in a-Si on the Electronic Density of States at the Band Edges", MRS Symp. Proc. **219**, 581 (1991).

M.J. Williams, C. Wang and G. Lucovsky, "A Comparative Study of the Light-Induced Defects in Intrinsic Amorphous and Microcrystalline Silicon Deposited by Remote Plasma Enhanced Chemical Vapor Deposition, International Meeting on Stability of Amorphous Silicon Materials and Solar Cells, AIP Conference Proceedings **234**, 211 (1991).

C. Wang, C.H. Bjorkman, D.R. Lee, M.J. Williams, and G. Lucovsky, "Deposition of Heavily Doped μc-silicon Thin Films by Remote Plasma-Enhanced Chemical Vapor Deposition Process (Remote PECVD)", MRS Symp. Proc. **204**, 227 (1991).

G. Lucovsky, "Local Bonding Arrangements and Vibrational Properties of Hydrogen Atoms in Amorphous Silicon Alloys", Rev. Roum. Phys. **36**, 659 (1991).

S.S. Kim, C. Wang, G.N. Parsons and G. Lucovsky. "a-Si:H Thin Film Transistors and Logic Circuits Fabricated in an Integrated Multichamber System", MRS Symp. Proc. **192**, 373 (1990). (not listed in 1990 report)

1992

D.R. Lee, Y. Ma, T. Yasuda, C.H. Björkman and G. Lucovsky, "Stacked-gates with doped μc-Si electrodes and SiO_2 dielectrics, both deposited by Remote PECVD", J. Vac. Sci. Technol **A10**, 788 (1992).

G. Lucovsky, C. Wang and Y.L. Chen, Barrier-limited Transport in μc-Si and μc-Si,C Thin Films Prepared by Remote PECVD", J. Vac. Sci. Technol **A10**, 2025 (1992).

J. Zing, J.L Whitten and G. Lucovsky, "Ab-Initio Calculations of Si-H Bond Energies," Phys. Rev. **B45**, 13978 (1992).

G. Lucovsky, "Hydrogen in Amorphous Silicon: Local Bonding and Vibrational Properties", J. Non-Cryst. Solids **141**, 241 (1992).

Y.L. Chen, C. Wang, G. Lucovsky, D.M. Maher and R.J. Nemanich, "Transmission Electron Microscopy and Vibrational Spectroscopy Studies of Undoped and Doped Si,H and Si,C:H Films", J. Vac. Sci. Technol **A10**, 874 (1992).

B.N. Davidson, S.M. Cho and G. Lucovsky, "Localized States in amorphous Si and Si,Ge alloys", AIP Conf. Proc. **269**, 369 (1992).

D.R. Lee and G. Lucovsky, "Work Function Difference Between n-type μc-Si Gate Electrodes Deposited by Remote PECVD and p-type c-Si Substrates in MOS Capacitors," MRS Symp. Proc. **258**, 979 (1992).

S. M. Cho, B. N. Davidson and G. Lucovksy, "Energy Differences Between the Si and the Ge Dangling Bond Defects in a-$Si_{1-x}Ge_x$ Alloys", MRS Symp. Proc. **258**, 583 (1992).

B. N. Davidson, G. Lucovsky and J. Bernholc, "Defect States and Structural Disorder in a-Si", MRS Symp. Proc. **258**, 263 (1992).

S. S. He, D. J. Stephens, Yi Ma, T. Yasuda, S. Habermehl and G. Lucovsky, "Control of Process Induced Defects in the Formation of Single and Multiple Layer Dielectric

Structures for Si Semiconductor Devices", MRS Symp. Proc. **262**, 653 (1992).

To be published in 1993

A. Esser, H. Heesel and H. Kurz, C. Wang, G.N. Parsons and G. Lucovsky, "Transport Properties of Optically-Generated Free Carriers in Amorphous Silicon, a-Si:H in the Femtosecond Time Regim", Phys. Rev. **B**15.

A. Esser, H. Heesel and H. Kurz, C. Wang, G.N. Parsons and G. Lucovsky, "Femtosecond Spectroscopic Study of Ultrafast Carrier Relaxation in Hydrogenated Amorphous Silicon a-Si:H", J. Appl. Phys.

G. Lucovsky, C. Wang, M. J. Williams, Y. L. Chen, and D. M. Maher, "Transport and Microstructure of Microcrystalline Si Alloys", MRS Symp. Proc. (1993).

S. S. He, D. J. Stephens, R. W. Hanmaker and G. Lucovsky, "Channel Layer Surface Modifications in a-Si:H Thin Film Transistors with Oxide/Nitride Dielectric Layers", MRS Symp. Proc. (1993).

W. A. Turner, M. J. Williams, Y. L. Chen, D. M. Maher, and G. Lucovsky, "Optical and Electrical Properties of Boron-Doped mc-Si Prepared by Reactive Magnetron Sputtering from c-Si Targets", MRS Symp. Proc. (1993).

S. Q. Gu, J. M. Viner, and P. C. Taylor, M. J. Williams, W. A. Turner, and G. Lucovsky, "Photoluminescence in B-Doped mc-Si:H", MRS Symp. Proc. (1993).

G. Lucovsky, Y. Ma, S. S. He, T. Yasuda, D. J. Stephens and S. Habermehl, "Quasi-Stoichiometric Silicon Nitride Thin Films Deposited at Low-Temperature by Remote PECVD", MRS Symp. Proc. (1993).

GRADUATE STUDENTS AND POST DOCTORAL FELLOWS

- PhD Degrees

  Parsons, C. Wang, S. Kim and B. Davidson

  Esser (RWTH-Aachen)

- Completing PhD Requirements

  Williams, S. Cho and SS He

- Post Doctoral Fellows

  Turner and Z. Jing

RECOMMENDATIONS FOR CONTINUED STUDY

It is recommended that research be continued in two areas:

- the development and evaluation of B-compensated μc-Si as a candidate material for the i-region of solar cells, and

- the development of a-Si,O:H and a-Si,N:H as candidate materials for the i-region of the wide band-gap cells in triiple tandem solar cell configurations.

Document Control Page	1. NREL Report No. NREL/TP-451-5452	2. NTIS Accession No. DE93017083	3. Recipient's Accession No.

4. Title and Subtitle
Fundamental Studies of Defect Generation in Amorphous Silicon Alloys Grown by Remote Plasma-Enhanced Chemical-Vapor Deposition

5. Publication Date
August 1993

6.

7. Author(s)
G. Lucovsky

8. Performing Organization Rept. No.

9. Performing Organization Name and Address
Department of Physics, Material Science and Engineering
North Carolina State University
Raleigh, NC 27695-8202

10. Project/Task/Work Unit No.
PV32110

11. Contract (C) or Grant (G) No.
(C) XM-9-18141-2
(G)

12. Sponsoring Organization Name and Address
National Renewable Energy Laboratory
1617 Cole Blvd.
Golden, CO 80401-3393

13. Type of Report & Period Covered
Technical Report
1 July 1989 - 31 December 1992

14.

15. Supplementary Notes
NREL technical monitor: J. Benner

16. Abstract (Limit: 200 words)
This report describes research to reduce the intrinsic bonding defects in amorphous and microcrystalline Si alloys by controlling the bonding chemistry and the microstructure via the deposition process reactions. The specific approach was to use remote plasma-enhanced, chemical-vapor deposition (PECVD) and reactive magnetron sputtering to limit the multiplicity of deposition reaction pathways, and thereby gain increased control over the thin-film chemistry and microstructure. The research included (1) the deposition of amorphous and microcrystalline Si alloy materials by the PECVD process and by reactive magnetron sputtering, and (2) the evaluation of the material properties of these films for potential applications in PV devices. The focus of the research was on gaining a fundamental understanding of the relationships between deposition reaction pathways, the bonding of dopant and alloy atoms, and the electrical properties of importance for PV applications. This involved studying the factors that contribute to defect generation and to defect removal and/or neutralization. In addition to the experimental studies, the research also included theoretical and modeling studies aimed at understanding the relationships between local atomic arrangements of Si and alloy atoms, and the electrical, optical, vibrational, and defect properties.

17. Document Analysis
a. Descriptors
amorphous silicon ; alloys ; deposition ; photovoltaics ; solar cells ; defects
b. Identifiers/Open-Ended Terms
c. UC Categories
271

18. Availability Statement
National Technical Information Service
U.S. Department of Commerce
5285 Port Royal Road
Springfield, VA 22161

19. No. of Pages
57

20. Price
A04

Form No. 0069E (6-30-87)